

RESEARCH ARTICLE

10.1002/2015JD023501

Key Points:

- First global ocean comparison of PARASOL SSA with observations and models
- PARASOL observes stronger aerosol absorption than models, larger in the tropics
- Direct aerosol radiative effect at TOA is overestimated by models

Correspondence to:

C. Lacagnina,
C.Lacagnina@sron.nl

Citation:

Lacagnina, C., O. P. Hasekamp, H. Bian, G. Curci, G. Myhre, T. van Noije, M. Schulz, R. B. Skeie, T. Takemura, and K. Zhang (2015), Aerosol single-scattering albedo over the global oceans: Comparing PARASOL retrievals with AERONET, OMI, and AeroCom models estimates, *J. Geophys. Res. Atmos.*, 120, 9814–9836, doi:10.1002/2015JD023501.

Received 10 APR 2015

Accepted 23 AUG 2015

Accepted article online 19 SEP 2015

Published online 30 SEP 2015

Aerosol single-scattering albedo over the global oceans: Comparing PARASOL retrievals with AERONET, OMI, and AeroCom models estimates

Carlo Lacagnina¹, Otto P. Hasekamp¹, Huisheng Bian², Gabriele Curci^{3,4}, Gunnar Myhre⁵, Twan van Noije⁶, Michael Schulz⁷, Ragnhild B. Skeie⁵, Toshihiko Takemura⁸, and Kai Zhang^{9,10}

¹SRON Netherlands Institute for Space Research, Utrecht, Netherlands, ²Joint Center for Earth Systems Technology, University of Maryland, Baltimore County, Catonsville, Maryland, USA, ³Department of Physical and Chemical Sciences, University of L'Aquila, L'Aquila, Italy, ⁴CETEMPS, University of L'Aquila, L'Aquila, Italy, ⁵Center for International Climate and Environmental Research - Oslo, Oslo, Norway, ⁶KNMI Royal Netherlands Meteorological Institute, De Bilt, Netherlands, ⁷Norwegian Meteorological Institute, Oslo, Norway, ⁸Research Institute for Applied Mechanics, Kyushu University, Fukuoka, Japan, ⁹Pacific Northwest National Laboratory, Richland, Washington, USA, ¹⁰Max Planck Institute for Meteorology, Hamburg, Germany

Abstract The aerosol single-scattering albedo (SSA) over the global ocean is evaluated based on polarimetric measurements by the PARASOL (Polarization and Anisotropy of Reflectances for Atmospheric Sciences coupled with Observations from a Lidar) satellite. For the first time, global ocean SSA and Absorption Aerosol Optical Depth (AAOD) from this instrument are shown and evaluated against other observations (the Aerosol Robotic Network, AERONET, and the Ozone Monitoring Instrument, OMI). The observational data sets compare reasonably well, with the majority of the colocated points within 0.05 of the AERONET measurements. PARASOL shows that SSA is characterized by high spatial and seasonal variability, also over the open ocean far from the inland emission regions. The near global coverage in the visible spectral range provided by the PARASOL retrievals represents a unique opportunity to evaluate aerosol optical properties simulated by global aerosol models, as performed in the Aerosol Comparisons between Observations and Models (AeroCom) framework. The SSA (AAOD) estimated by the AeroCom models is generally higher (smaller) than the SSA (AAOD) retrieved from PARASOL. On the other hand, the mean simulated aerosol optical depth is consistent or slightly underestimated compared with observations. An overestimate of the aerosol scattering, compared to absorption, by the models would suggest that these simulate an overly strong aerosol radiative cooling at top of atmosphere, over most of the ocean surfaces. This implies that aerosols have a potentially stronger direct and semidirect impact within the atmosphere than currently simulated.

1. Introduction

Atmospheric aerosols influence the Earth's energy budget by scattering and absorbing radiation ("direct effect") and in multiple other ways, for instance by perturbing the albedo of clouds and their lifetime ("indirect effect"). Estimates of both effects are hampered by large uncertainties and make the largest contribution to the overall uncertainty in the radiative forcing causing climate change [Myhre *et al.*, 2013b].

The former effect, referred to as the direct radiative effect of aerosols (DREA), can be calculated based on the difference between radiative fluxes in the absence and presence of aerosols [Loeb and Manalo-Smith, 2005]. Negative (positive) values of DREA at top of atmosphere (TOA) indicate that the climate system is cooled (warmed) by the aerosols. Radiative perturbations within and below the aerosol layers are also relevant to climate, because these can affect the temperature structure of the atmosphere, cloud formation, and persistence ("semidirect effect") [e.g., Hansen *et al.*, 1997]. In absence of clouds, DREA depends on the aerosol optical properties, primarily optical depth (AOD) and single scattering albedo (SSA), and on the surface albedo. The columnar AOD quantifies the total extinction of a light beam interacting with aerosols and is related to their amount. The SSA, defined as the ratio of the scattering to the total attenuation, provides an indication of the relative abundance of absorbing aerosol components. Generally, purely scattering aerosols (e.g., sea salt) enhance the backscattering of solar radiation to space, resulting in negative DREA, i.e., cooling effect.

For absorbing aerosols (e.g., black carbon, BC) a decrease of SSA can change the sign of DREA from negative (cooling) to positive (warming), depending on the albedo of the underlying surface [Russell *et al.*, 2002]. Therefore, AOD and SSA are crucial parameters controlling the radiative impact of the aerosols. Myhre *et al.* [2009] and Loeb and Su [2010] pointed out that insufficient accuracy of SSA estimates accounts for much of the uncertainties in DREA calculations.

Because of its fundamental importance, space-based remote sensing techniques to retrieve SSA have been increasingly developed. At present, three main satellite products provide specifically this information over ocean. First, the Ozone Monitoring Instrument (OMI) onboard NASA's Aura satellite measures the solar light scattered by the atmosphere, which is then used to derive aerosol optical depth (AOD) and absorption AOD (AAOD) [Torres *et al.*, 2013]. The retrieval of SSA from OMI-Aura is limited to the UV range. Second, the Multiangle Imaging Spectroradiometer (MISR) flying on the Terra spacecraft uses multiple camera views to retrieve aerosol optical properties [Kahn *et al.*, 2005]. Currently, MISR SSA retrievals cannot be considered quantitative, because of limitations in the range of components and mixtures available in the operational algorithm and in part due to limited information content in the MISR data itself [Chen *et al.*, 2008; Kahn *et al.*, 2010]. However, qualitative SSA distinctions can be made when minimum AOD and surface quality conditions are met. Third, the Polarization and Directionality of Earth Reflectances [Deschamps *et al.*, 1994] instrument on board the PARASOL (Polarization and Anisotropy of Reflectances for Atmospheric Sciences coupled with Observations from a Lidar) Sun-synchronous microsatellite provides multiangle multispectral photopolarimetric measurements. This type of observations has notably higher sensitivity to the details of aerosol and surface characteristics, compared to intensity-only retrievals, and thus provides aerosol microphysical properties with high accuracy [Mishchenko and Travis, 1997; Chowdhary *et al.*, 2001; Hasekamp and Landgraf, 2007].

Full use of the information supplied by PARASOL is made possible using novel retrieval algorithms that consider a continuous space of aerosol properties [Hasekamp *et al.*, 2011; Dubovik *et al.*, 2011], in contrast to the more traditional standard aerosol retrieval approach. In this study we use the PARASOL observations processed with the algorithm described in detail by Hasekamp *et al.* [2011]. A recent work by Russell *et al.* [2014] has employed the same data to successfully classify various aerosol types. Here we run this algorithm for 1 year (2006), exploring global clear-sky ocean coverage SSA that is, for the first time, available from polarimetric measurements. The resulting aerosol optical properties are evaluated against ground-based measurements (section 3) and compared with OMI-Aura observations in section 4. In the second part of this study (section 5), the novel PARASOL products are used to evaluate aerosol optical properties simulated by various global aerosol models, participating in the AeroCom (Aerosol Comparisons between Observations and Models) project. AeroCom is an international effort that documents differences of global aerosol models and assembles data sets for aerosol model evaluations [Schulz *et al.*, 2009]. Finally, in section 6 we present our concluding remarks.

2. Data

We process (i.e., interpolate and regrid) daily mean values of AOD and AAOD from different sources for year 2006. The SSA is then computed as

$$SSA = \frac{AOD - AAOD}{AOD} \quad (1)$$

2.1. PARASOL

PARASOL provides aerosol properties by performing multiangle, multispectral photopolarimetric measurements at (up to) 16 viewing geometries in nine spectral bands ranging from 0.44 to 1.02 μm . Aerosol retrievals are performed at $18 \times 18 \text{ km}^2$ resolution with nearly global coverage in 2 days. For this study Collection 2 of the PARASOL L1B data is used. The combination of spectral-directional and polarized signature supplies a very strong constraint to invert the aerosol load and characteristics. The derived column atmosphere aerosol properties are generated employing an improved version of the Hasekamp *et al.* [2011] algorithm, for clear-sky conditions in 2006 over the oceans. Improvements in the algorithm include the consideration of nonspherical particles for the coarse mode and the use of more spectral bands, from two (0.49 and 0.67 μm) to four (0.49, 0.67, 0.86, and 1.02 μm unpolarized). The retrieved parameters at these four wavelengths are then reported at the remaining PARASOL bands, assuming the complex refractive index being independent of wavelength.

Table 1. General Description of the AeroCom Models Used in This Study

Model	Type	Resolution (Longitude × Latitude)	Vertical Levels	Aerosol Mixing	Responsible	References
ECHAM5-HAM2	GCM	1.8° × 1.8°	31	Ext mix of int modes	Kai Zhang	Zhang <i>et al.</i> [2012]
GEOS-Chem-v822	CTM	2.5° × 2.0°	47	Ext	Gabriele Curci	Bey <i>et al.</i> [2001]
GMI	CTM	2.5° × 2.0°	31	Ext	Huisheng Bian	Liu <i>et al.</i> [2007]
GOCART-v4	CTM	2.5° × 2.0°	30	Ext	Thomas Diehl	Chin <i>et al.</i> [2000]
OsloCTM2-v2	CTM	2.8° × 2.8°	60	Ext, partly int for BC	Gunnar Myhre	Myhre <i>et al.</i> [2007]
SPRINTARS-v385	GCM	1.1° × 1.1°	56	Ext, int for hydrophilic BC	Toshihiko Takemura	Takemura <i>et al.</i> [2005]
TM5-v3	CTM	3.0° × 2.0°	34	Ext mix of int modes	Twan van Noije	van Noije <i>et al.</i> [2014]

Finally, a quality filter is applied to the retrieval results based on a goodness-of-fit criterion between measured and modeled radiances, with $\chi^2 < 10$. The quantity χ^2 is defined as $\chi^2 = \left[\sum_{i=1}^N (y_i - F_i)^2 / \sigma_i^2 \right] / N$, where N is the number of measurements, F_i stands for the forward model vector element i , y_i is the measurement vector element i , and σ_i the corresponding uncertainty. This filter has also the effect of disregarding cloud-contaminated pixels, as described in detail in Stap *et al.* [2014]. The resulting retrieval pixels of AOD and AAOD are averaged, using their median values, on a global grid. SSA is then computed based on these two quantities.

2.2. AERONET

Aerosol Robotic Network (AERONET) is a worldwide network of automatic Sun- and sky-scanning ground-based measurements [Holben *et al.*, 2001]. Column-integrated SSA is retrieved at four wavelengths ranging from 0.44 to 1.02 μm , while AOD is reported on more bands [Dubovik and King, 2000]. The estimated accuracy of this data set is within ± 0.01 and ± 0.02 for AOD and AAOD and generally within ± 0.03 for SSA associated with AOD_{0.44} larger than 0.4 [Dubovik *et al.*, 2000; Mallet *et al.*, 2013]. We primarily use the AERONET version 2 level 2.0 product, which reports cloud screened and quality assured data. When needed, analyses using level 1.5 are also shown. Unlike level 2.0, level 1.5 reports SSA also for AOD_{0.44} ≤ 0.4 , which increases significantly the number of collocated points between PARASOL and AERONET. It should be noticed that larger uncertainties for SSA ($> \pm 0.03$) are expected at low AODs. The level 1.5 product is similar to level 2.0, but data are not quality assured. Several preprocessing and postprocessing criteria were required for both levels, more stringent for the latter. Data from level 1.5 are used here with the additional criterion that the solar zenith angle must be $\geq 50^\circ$ (as is the case for level 2.0).

2.3. OMI-Aura

In this study the OMAERUV Level 2 Collection 003 V1.4.2 product [Jethva *et al.*, 2014] is used as an independent data set, providing the global pattern of SSA. The information on aerosol absorption in OMI measurements comes, to a large extent, from the interaction with Rayleigh scattering in the UV spectral region [Torres *et al.*, 2013]. In this data set AOD and AAOD are derived based on the reflectances measured by the OMI instrument onboard the Aura spacecraft at 0.39 μm . The retrieved parameters are also reported at 0.35 μm and 0.50 μm . We use only values over the ocean associated with the algorithm quality flag 0, which are considered to be the best in accuracy.

2.4. AeroCom Models

We use data from seven models contributing to the AeroCom phase II intercomparison project experiment A2-CTRL-06 [Schulz *et al.*, 2009]. These are the seven models with daily output available in the AeroCom portal for this type of experiment. Models were run in their standard configurations, constrained by meteorological conditions for year 2006 and prescribed aerosol precursors emissions for 2006 or previous years. The emission data sets are based on modelers' choices. Table 1 gives an overview of the models used (see Myhre *et al.*, 2013a, for more details on the model characteristics). Daily outputs from the AeroCom models were regridded onto a $3^\circ \times 2^\circ$ regular longitude \times latitude grid, which is the coarsest native grid among the models analyzed.

In order to make a fair comparison with the AeroCom models, PARASOL observations are regridded onto the same $3^\circ \times 2^\circ$ grid and interpolated at the same wavelength (0.55 μm). The AOD and AAOD are interpolated by natural log function using the nearest available wavelengths. SSA is then computed based on these two

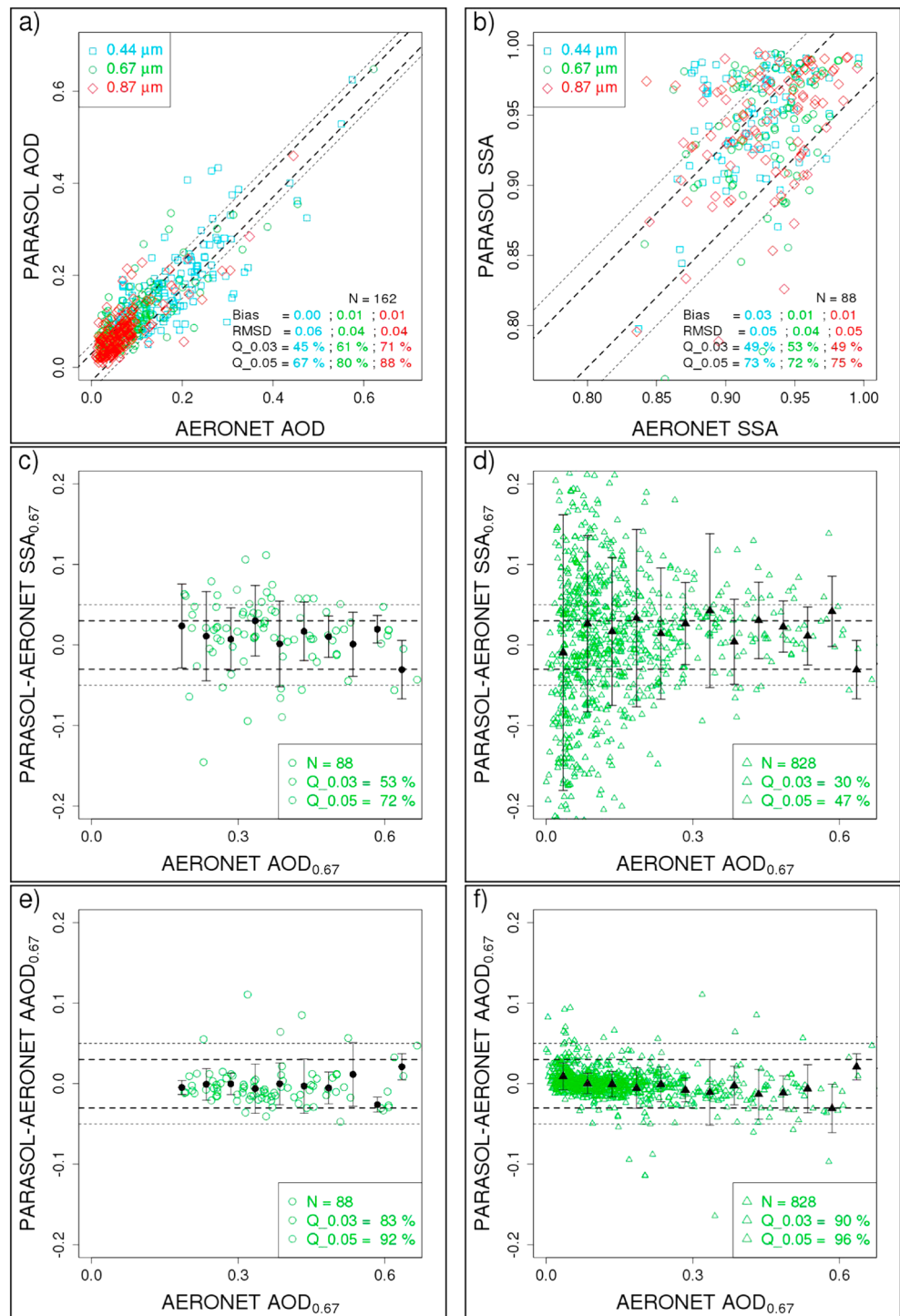


Figure 1. Various aerosol optical properties derived from colocated observations of AERONET level 2.0 and PARASOL for the year 2006. Colocated points are identified when the distance between the measurements is less than 55 km and within 1 h for AOD and within 3 h for SSA and AAOD. Triangles indicate quantities derived using AERONET level 1.5. The percentage of the number of colocated points (N) falling within the absolute difference PARASOL-AERONET of 0.03 and 0.05 is indicated by $Q_{0.03}$ and $Q_{0.05}$, respectively, and delimited by dashed lines in each panel. (a) AOD from AERONET versus AOD from PARASOL at different wavelengths. The root-mean-square deviation (RMSD) and bias (PARASOL-AERONET) are also shown. (b) Similar to Figure 1a but for SSA. (c) AERONET AOD versus SSA difference PARASOL-AERONET at $0.67 \mu\text{m}$, black points are the mean of the difference for each AOD interval of 0.05, along with 1σ standard deviation. (d) Similar to Figure 1c, but AERONET level 1.5 is used. (e and f) Similar to Figures 1c and 1f, respectively, but for AAOD.

quantities. Sample differences are eliminated by considering only daily model outputs where PARASOL data are available.

3. Evaluation of PARASOL-Derived Aerosol Optical Properties

The AERONET data set provides the benchmark for the PARASOL evaluation. Coincident points between the two observations are identified when the distance is less than 55 km and within a time window of ± 1 h for AOD and ± 3 h for SSA.

Figure 1a shows AOD from the colocated PARASOL and AERONET points at their original wavelengths. The statistical scores reveal very good agreement between the two data sets, which is better at longer wavelengths. More than two thirds of the PARASOL AOD points are found to be within the absolute difference of ± 0.05 with AERONET AOD. Robust agreement between the two observations is also found for SSA (Figure 1b). PARASOL exhibits a small positive bias, which is reduced at longer wavelengths. Overall, PARASOL observations appear able to capture the spectral variability of SSA and AOD, typical of smoke, mineral dust, and industrial aerosols.

Since at large aerosol loading the inversion algorithm used in AERONET is expected to be more robust and accurate, due to stronger absorption signal, we calculate the absolute difference in SSA between PARASOL and AERONET as a function of AERONET AOD_{0.67} (Figure 1c). It shows that the mean of differences between the two sensors is within the known uncertainty of AERONET for any AOD bin, i.e., ± 0.03 . Most of the PARASOL individual points (about three fourth) agree within ± 0.05 of the AERONET SSA. The sample of the colocated PARASOL-AERONET SSA observations is particularly small, because AERONET level 2.0 reports SSA only when AOD_{0.44} > 0.4, limiting strongly the comparison over the oceans. For this reason we show results obtained with AERONET level 1.5 in Figure 1d. The spread of the differences between the two observational data sets is larger for lower AODs, but the mean of the differences remains within the ± 0.05 uncertainty level. As far as AAOD is concerned, Figures 1e–1f show that the majority of points representing the difference between the two measurements is within ± 0.03 for both AERONET levels 2.0 and 1.5. The differences become somewhat larger with increasing AOD. We attribute this to the fact that high-AOD events are concentrated in plumes and thus are less homogeneous than lower AOD cases. As a result, the spatiotemporal averaging is likely affected by more sampling-related discrepancies.

The geolocation of the coincident AERONET-PARASOL points in Figures 1a–1c and 1e is shown in Figure 2, yearly averaged. The colocated values of AOD from PARASOL are often very similar to the AERONET AODs and do not exhibit significant bias (Figure 2a). In line with the ground-based observations, PARASOL captures regional changes in aerosol load. For instance, point locations close to North Africa, Arabian Peninsula, and eastern China identify major aerosol source regions, while the point locations in the Southern Hemisphere exhibit low AODs, associated with more pristine environments. Regarding SSA, PARASOL compares favorably with AERONET and is well capable to reproduce a reasonable SSA range between 0.8 and 1.0 (Figure 2b). Very close agreement is found in North America and Korean peninsula. In the other point locations, notably in Europe, PARASOL tends to overestimate SSA. Figure 3 shows RMSD and the number of colocated points contributing to the annual means in Figure 2.

Discrepancies between the two data sets may arise from uncertainties specific of the PARASOL and AERONET observations, from the intrinsic differences between the instruments and in the diagnostics used to compare them. AERONET AOD is derived exclusively from direct-Sun extinction measurements several times per day, while AERONET SSA is retrieved through a combination of direct-Sun and sky-scan data associated with approximately 5 km radius region around the measurement station [Dubovik and King, 2000]. On the other hand, PARASOL acquires data about once a day over a much larger area (18×18 km²). As a result, the primary uncertainty in this evaluation arises from sampling differences. In addition, satellite retrievals over ocean are always further away from the land and thus from the main pollution sources than AERONET sites. The underlying assumption (in the comparison with AERONET) is that the aerosol properties are uniform within 55 km away from the coast. Moreover, different constraints characterize the retrieval algorithms in AERONET and PARASOL. The former assumes 22 size bins for size distribution and the refractive index does not depend on size, whereas the latter assumes a bimodal approach and the refractive index can differ with size modes. Other uncertainties include differences in the instrument calibration and intrinsic information content of the measurements.

As far as PARASOL-related uncertainty is concerned, despite multiangle measurements facilitating the screening of cloud-contaminated pixels, thin cirrus can bias the aerosol product [Tanré et al., 2011]. Given the size

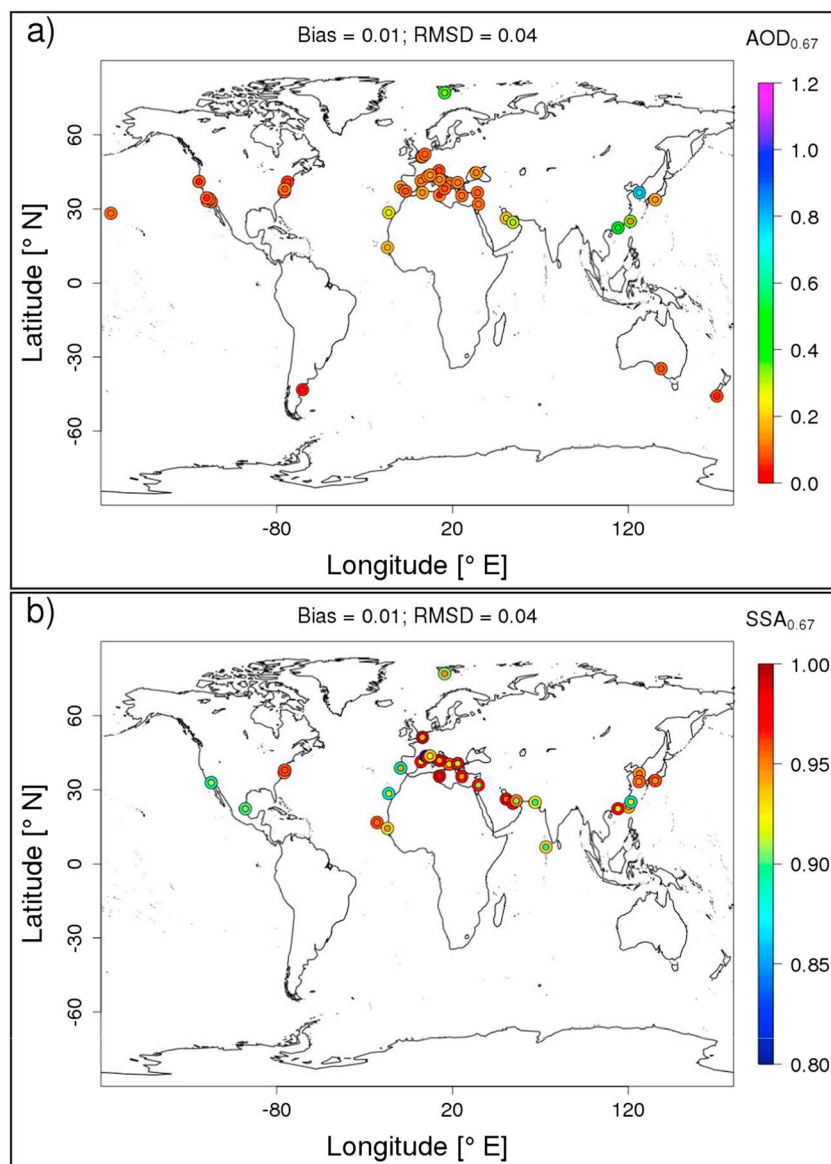


Figure 2. Annual mean distribution of (a) AOD and (b) SSA at $0.67 \mu\text{m}$ derived from the collocated AERONET level 2.0 (inner circles) and PARASOL (outer circles) points in Figures 1a and 1b. Bias (PARASOL-AERONET) and root-mean-square deviation (RMSD) are shown at the top of each panel. The point locations in Figures 2a and 2b should not be expected to be the same, because of the different time windows selected in the collocation procedure and because of the more stringent filtering criteria applied in AERONET for SSA than for AOD.

of the $18 \times 18 \text{ km}^2$ footprint, subpixel clouds cannot be completely avoided and the goodness-of-fit criterion used to flag successful retrievals may not exclude thin cirrus [Stap *et al.*, 2014]. Additional sources of uncertainty may arise from the assumptions in the retrieval algorithm, such as the assumed aerosol layer height and the approximation of wavelength independence of the complex refractive index.

Despite being among the best data sets for this type of analysis, the AERONET measurements themselves bring a certain degree of uncertainty. The AERONET SSA is expected to be accurate within ± 0.03 [Dubovik *et al.*, 2000]. Many researchers found good agreement within this uncertainty between AERONET and in situ data [Johnson *et al.*, 2009; Schafer *et al.*, 2014]. However, other studies comparing airborne in situ measurements with AERONET SSA documented larger discrepancies by more than 0.04 [Leahy *et al.*, 2007; Osborne *et al.*, 2008]. Finally, validating PARASOL SSA over ocean is challenging, because of the very few coincident events meeting the AERONET high AOD and high solar zenith angle acceptance criteria. Longer time series than the single year used in this study would help to acquire better statistics to average out sampling anomalies.

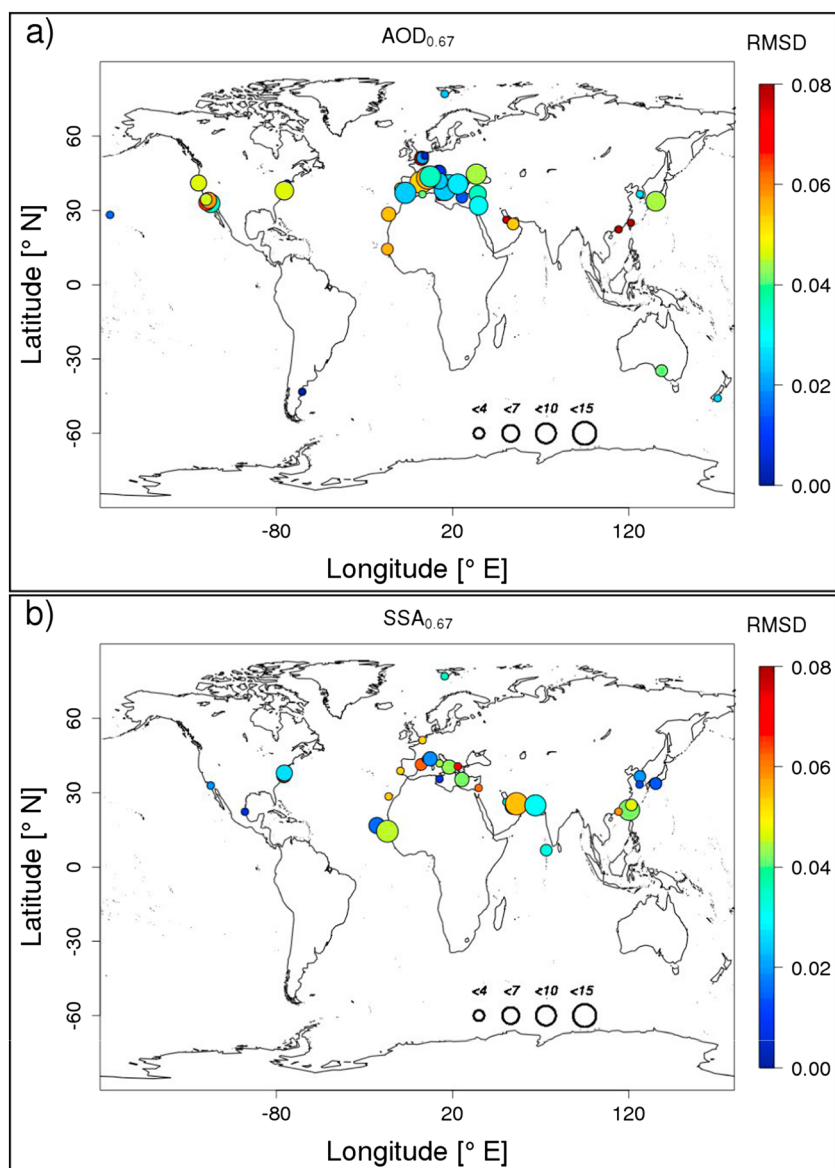


Figure 3. As for Figure 2 but the color scale represents the root-mean-square deviation (RMSD) between AERONET and PARASOL at each station. The size of the circles represents the number of collocated measurements, as indicated in the legend.

In conclusion, bearing in mind the fundamentally different ground-based and spaceborne approaches, the PARASOL and AERONET results can be considered in close agreement within the uncertainty in the sensors and diagnostics.

4. Spatial Patterns of Aerosol Optical Properties

The PARASOL retrieval measurements are now shown on a $1^\circ \times 1^\circ$ grid. The $AOD_{0.44}$ map (Figure 4a) depicts a well-known pattern, with maxima associated with the major aerosol emissions from Africa and Eastern Asia, followed by plumes of particles due to atmospheric transport in the downwind direction. The magnitude and distribution of AOD is in line with observations based on the other main satellites [cf. *Remer et al., 2009*].

For the first time, global coverage SSA based on polarimetric measurements is available and shown in Figure 4b. The oceanic $SSA_{0.44}$ map from PARASOL exhibits a very different pattern from that of AOD. By definition, SSA is independent of the aerosol load and can be regarded as a proxy for the aerosol relative composition. Most of the aerosol absorption is from BC and, to a lesser extent, from organic matter and dust.

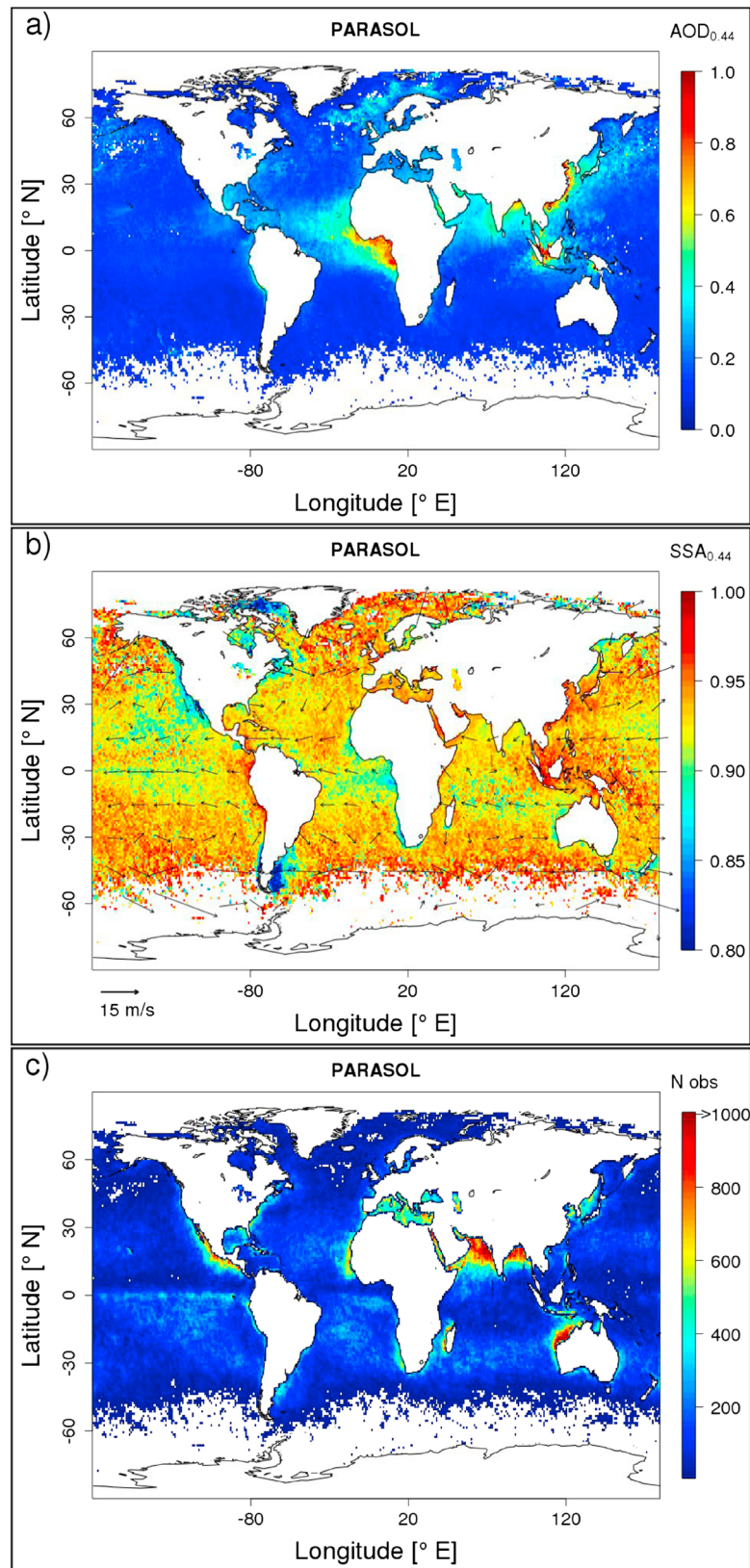


Figure 4. Annual mean distribution of PARASOL (a) AOD and (b) SSA at 0.44 μm and (c) number of observations for year 2006. Grid boxes filled with less than 5 pixels in the annual mean are screened out. Arrows are the annual mean wind direction and strength at 850 hPa from ERA-Interim reanalysis [Dee *et al.*, 2011].

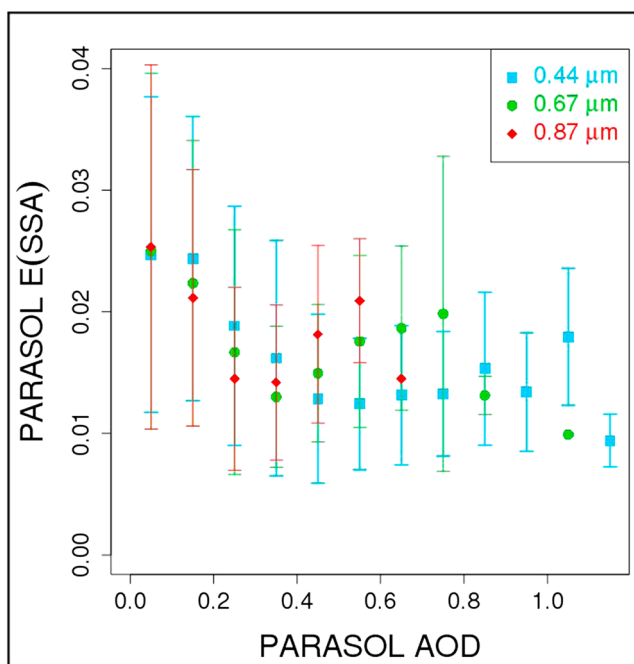


Figure 5. Mean of the PARASOL retrieval error as a function of AOD intervals of 0.1, along with 1σ standard deviation, at different wavelengths.

Biomass burning regions are important sources of absorbing aerosols, where typical values of SSA range between 0.80 to 0.95 [Abel *et al.*, 2003; Eck *et al.*, 2013; Sayer *et al.*, 2014]. Observations detect the highest SSAs in the Southern Oceans at extratropical latitudes, where sea salt is dominant. In contrast, lower values around 0.90 are found west of the continents in the subtropics. This appears related with the transport to the adjacent oceans of absorbing fine particles originating from biomass burning, soil matter, and industrial pollution in western North America, South America, central and southern Africa and Australia. The annual mean wind at 850 hPa (Figure 4b) supports the argument that due to persistent large-scale circulation conditions, such as those associated with the trade winds, absorbing aerosol plumes substantially influence SSA, also far away from their emission sources. Along the intertropical convergence zone in the Pacific Ocean, SSA rises to higher values, likely associated with the strong water uptake taking place in these humid environments, typical of deep convective regimes. Deep convective conditions are also typical in the Indonesian region [e.g., Lacagnina and Selten, 2013]. This area is characterized by extensive fires contributing to much of the local aerosol emissions [e.g., Gras *et al.*, 1999]. Indeed PARASOL detects high AODs (Figure 4a) but also relatively high values of SSA (Figure 4b), despite smoke being expected to be generally strongly absorbing. The higher SSA detected by PARASOL over Indonesia, compared to other biomass burning regions, is consistent with the findings of Gras *et al.* [1999] and Sayer *et al.* [2014]. They noticed that the Indonesian smoke is significantly less absorbing than the adjacent smoke from Australia, because of different combustion phases and material burnt. Moreover, the typical high humidity characterizing the Indonesian area may also contribute to moderate low SSAs, through water uptake processes. On the other hand, the typical cloudy conditions characterizing this area decrease sensibly the number of clear-sky pixels observed by PARASOL, and some scenes identified as cloud-free may also be affected by subpixel cirrus, biasing the PARASOL retrievals. In addition, sampling differences among the grid boxes lead adjacent areas to be represented by different data, hence different aerosol events. The distribution of the number of observations is shown in Figure 4c.

Other features peculiar of the PARASOL SSA map are the remarkably low values (< 0.85) west of Greenland, in part due to pyrogenic carbon emissions across Canada [French *et al.*, 2008], and around the Patagonian region, in part owing to the transport of dark soil dust in that area [Prospero *et al.*, 2002; Ginoux *et al.*, 2004]. We do not have a clear explanation about why the retrieval algorithm should fail specifically in these small regions. The very low aerosol loadings, typical in these areas (Figure 4a), may affect the retrieval results, because of the low aerosol contribution to the radiative fluxes observed from space. However, this would not explain a systematic low scattering only for these areas. Straightforward solutions, such as processing retrievals with

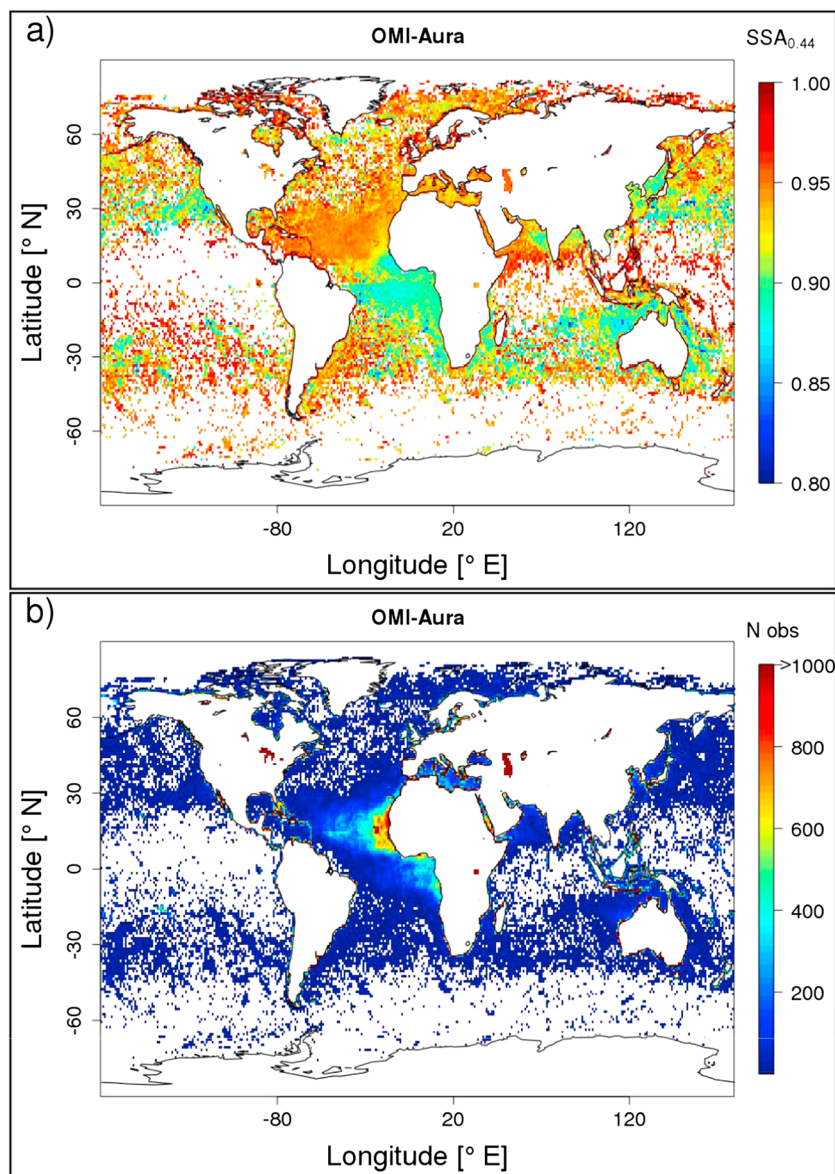


Figure 6. Annual mean distribution of OMI-Aura SSA at (a) 0.44 μm and (b) number of observations for year 2006.

more stringent quality filters (e.g., lower χ^2 thresholds) or setting a larger minimum number of pixels required for filling a grid box, do not change these peculiarities and reduce the global coverage of the data (not shown).

Finally, the Hasekamp *et al.* [2011] algorithm provides the retrieval error of various aerosol parameters, which can be used to assess the uncertainty of the PARASOL measurements. Since the retrieval of aerosol microphysical properties from space is expected to be more robust at large aerosol loading, Figure 5 shows the mean retrieval error of SSA as a function of AOD at different wavelengths. The retrieval error is within reasonable limits for any AOD bin but decreases sharply for AOD > 0.2, suggesting that PARASOL retrievals are more accurate closer to the aerosol emission sources, where the aerosol loading is the largest.

4.1. Comparing PARASOL and OMI-Aura SSA

In order to get more insights into PARASOL SSA, we now inspect global maps from an other independent data set with larger spatial coverage than AERONET, namely the OMI-Aura satellite observations (Figure 6). We calculate SSA through AOD and AAOD interpolated to 0.44 μm by natural log function, using the nearest available wavelengths. Exact agreement between PARASOL and OMI-Aura is not expected, because of sampling differences (different filtering criteria, compare Figure 4c with Figure 6b) and because of relevant differences

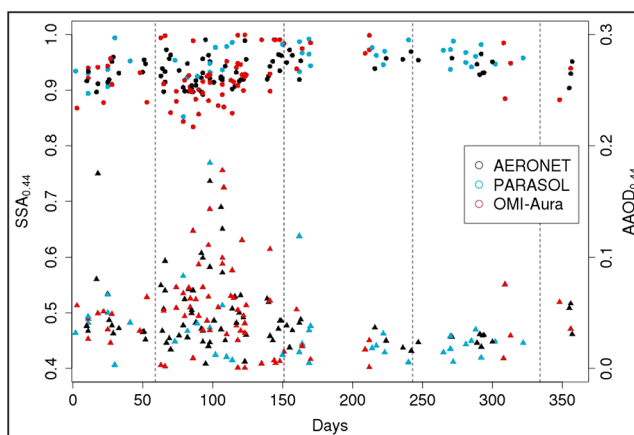


Figure 7. Comparison of daily SSA (dots) and AAOD (triangles) at $0.44 \mu\text{m}$ provided by AERONET, PARASOL, and OMI-Aura during 2006. As in AERONET, only events associated with $\text{AOD} > 0.4$ are considered. Measurements are collocated in space (within 55 km), but not in time. The three sites used are localized in Figure 2b between Korea and Japan (labeled in AERONET as “Gosan_SNU,” “Anmyon,” and “Shirahama”). Dashed lines delimit the different meteorological seasons.

in the retrieval algorithms and in the information content of the observations. These include the completely different spectral windows used (visible in the former versus near UV in the latter) and the different measurements (multiangle polarimetric versus intensity only, more details in section 2). It is worth noting that because of the difficulty in distinguishing the ocean color effects from those of low aerosol concentrations in the UV spectral range, OMI-Aura reports observations over the oceans only when absorbing aerosols (dust is also strongly absorbing in the UV window) are present in sufficient amounts [Torres *et al.*, 2013]. Therefore, the OMI-based method has a preference for strong aerosol events of, for example, desert dust outbreak and biomass burning [Veihelmann *et al.*, 2007]. Furthermore, OMI-Aura is based on intensity-only measurements; hence, more information needs to be prescribed (according to location and month of the year) in the retrieval algorithm, compared to PARASOL.

Figures 4b–6a show similarities and differences, but both reveal the rich structure of SSA, due to local differences in the aerosol composition. Both observational data sets detect similar emission sources of absorbing aerosols. These areas are often associated with biomass and fuel burning, such as in India [Duncan *et al.*, 2003], the Sahel and central Africa [Yang *et al.*, 2013], northern Australia [Gras *et al.*, 1999], and California [Cazorla *et al.*, 2013]. These absorbing plumes are transported in the downwind direction and diluted by mixing with other, more scattering, aerosol types. Furthermore, these absorbing particles undergo water uptake and aging processes, becoming more and more scattering, depending on the ambient humidity levels. In the tropical free-troposphere, wet removal and relative humidity are much lower in subsidence regimes than in deep convective areas. These mechanisms are largely consistent with the lower SSAs detected over most of the subtropical oceans and higher SSAs in the convergence zones in both the observational data sets. Moreover, the aerosols downwind of the Sahara, and the Arabian peninsula are primarily mineral dust leaving the deserts. Consistently, both PARASOL and OMI-Aura show scattering plumes in these areas, stronger for the latter instrument.

Notable disagreement is found off the coasts of Northeast Asia and further away in the North Pacific, around 35°N , where PARASOL observes larger SSA values. This region is characterized by a complex environment of aerosols, where dust and sea salt mix with local sulfate and BC pollution generated from vehicle emissions, coal burning, and industrial activities [Eck *et al.*, 2005]. As a result, a mixture of fine, coarse, absorbing, and scattering particles gives rise to a challenging environment for remote sensing observations. A more detailed comparison for this area is shown in Figure 7. Daily measurements from the different sensors are collocated in space (within 55 km), but not in time. The SSA and AAOD trends depicted by PARASOL and OMI-Aura are in reasonable agreement with AERONET. PARASOL is well capable to detect peaks of strong absorption, but many values associated with an important aerosol event in spring have been filtered out by the goodness-of-fit criterion. Analyses with more loose quality filters, show that the points screened out are associated with high AOD and often low SSA in PARASOL (not shown). This suggests that some data indicating high aerosol load

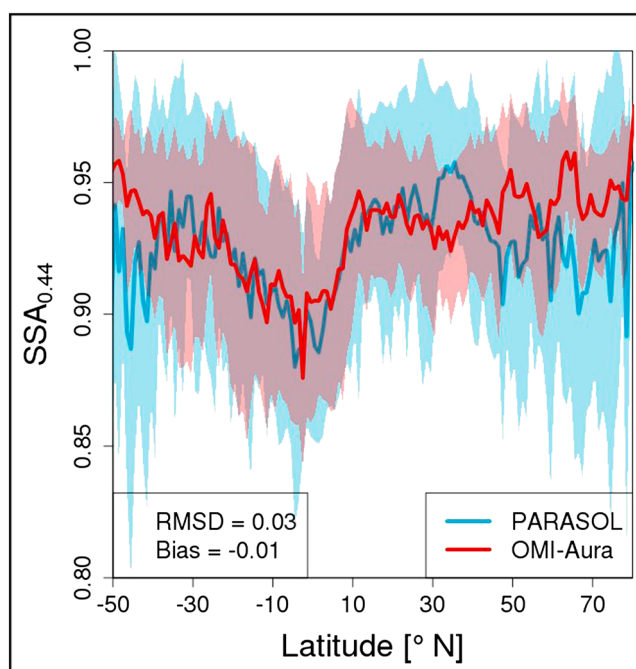


Figure 8. Zonal means of PARASOL and OMI-Aura observations in Figures 4b and 6a but considering only daily retrievals where both data sets are available. The shaded area represents the standard deviation of the zonal means. The root-mean-square deviation (RMSD) and bias (PARASOL-OMI-Aura) are also shown.

are dismissed. This partly explains the higher mean SSAs in Figure 4b than in Figure 6a. An other possibility is that the prescribed aerosol information (according to climatology) in the OMI-Aura algorithm is not optimal for this location. *Veihelmann et al.* [2007] pointed out that this constraint is very loose and has a preference for biomass burning aerosols. Eastern Asia experienced a strong increase of nitrogen and sulfate during 2006 with respect to the previous years [*Zhang et al.*, 2009; *Lamsal et al.*, 2011]. This may result in higher than expected aerosol scattering in this region.

In order to minimize sampling differences between PARASOL and OMI-Aura observations, Figure 8 shows the zonal means of the SSA distribution displayed in Figures 4b and 6a but considering only retrievals available simultaneously in both data sets. Despite both satellites being separated by a few minutes along their flight tracks, the different filtering criteria and retrieval techniques leave few coincident points. As a result, the zonal mean trends appear very scattered, particularly at higher latitudes. However, PARASOL and OMI-Aura observations compare favorably and exhibit the closest agreement over the tropical belt.

5. Comparison of PARASOL Observations With AeroCom Models

The global coverage provided by PARASOL in the midvisible range represents a unique opportunity to compare observed SSA and AAOD with values simulated by global aerosol models, as performed in the AeroCom framework.

Figure 9a shows the spatial variation of SSA retrieved by PARASOL. A striking feature is that absorbing aerosols substantially influence SSA over the ocean far away from their emission sources. This feature is not captured by the AeroCom models (Figure 9b), where SSA is low only close to the emission sources. The SSA values in the Bay of Bengal and central-west Africa are the most consistent between observations and simulations. Higher SSAs are found in the Southern Ocean, where sea salt is dominant, both in PARASOL and in the models. Overall, the spatial distribution of SSA is pretty uniform in the models and exhibits values higher than in PARASOL. Lower values are found in the area over Indonesia and off coasts of China. As discussed above, the area close to Patagonia and west of Greenland have very small SSAs that are unexpected and might be associated with retrieval artifacts. However, these low values are of marginal importance from a radiative perspective, given the associated low AOD and high latitude.

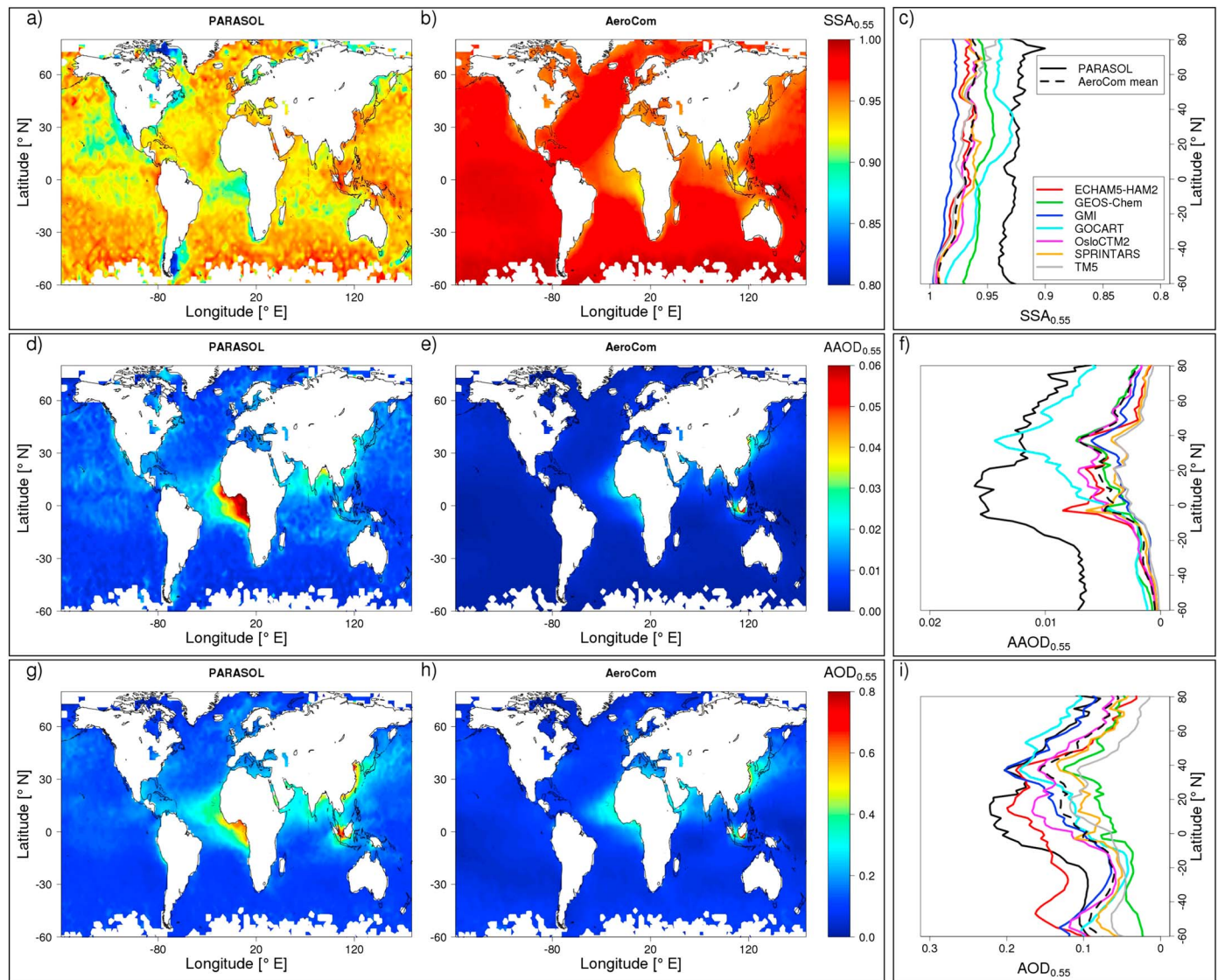


Figure 9. Annual mean distribution of (a–c) SSA, (d–f) AAOD, and (g–i) AOD at 0.55 μm for year 2006, from (Figures 9a, 9d, and 9g) PARASOL and (Figures 9b, 9e, and 9h) AeroCom models mean. (Figures 9c, 9f, and 9i) Zonal means of the individual AeroCom models and PARASOL. Grid boxes filled with less than 10 pixels in the annual mean are screened out.

The radiative impact of the differences between PARASOL and AeroCom models can be better interpreted by inspecting the AAOD maps (Figures 9d–9f). In general, satellite retrievals attest stronger AAOD than the models at all latitudes, with larger discrepancies in the tropics. However, these differences can be either positive or negative at the regional scale. The PARASOL AAOD exhibits a clear maximum close to central-west Africa, with plumes extending further offshore. AeroCom models simulate weaker and less extended AAOD. Large biases in this region were also found by *Kinne et al.* [2006]. Opposite departures are present over Indonesia. Both regions are dominated by biomass burning, but smoke optical properties are known to be different [*Eck et al.*, 2013; *Gras et al.*, 1999]. Since models specify the same optical properties of organic carbon all over the globe, PARASOL-AeroCom differences suggest that simulations do not capture the diversity of smoke in these regions. Other large departures between AeroCom models mean and PARASOL AAOD are found close to India, where the retrievals reveal stronger aerosol absorption. It is worth noting that the strips of low PARASOL SSA in the subtropics (Figure 9a) are negligible in the related AAOD map (Figure 9d), indicating that the radiative impact of these aerosols is small.

PARASOL and AeroCom models mean AAOD report similar values off the coasts of China, while SSA is much higher in the retrievals. This indicates smaller values of simulated AOD than observed, as shown in

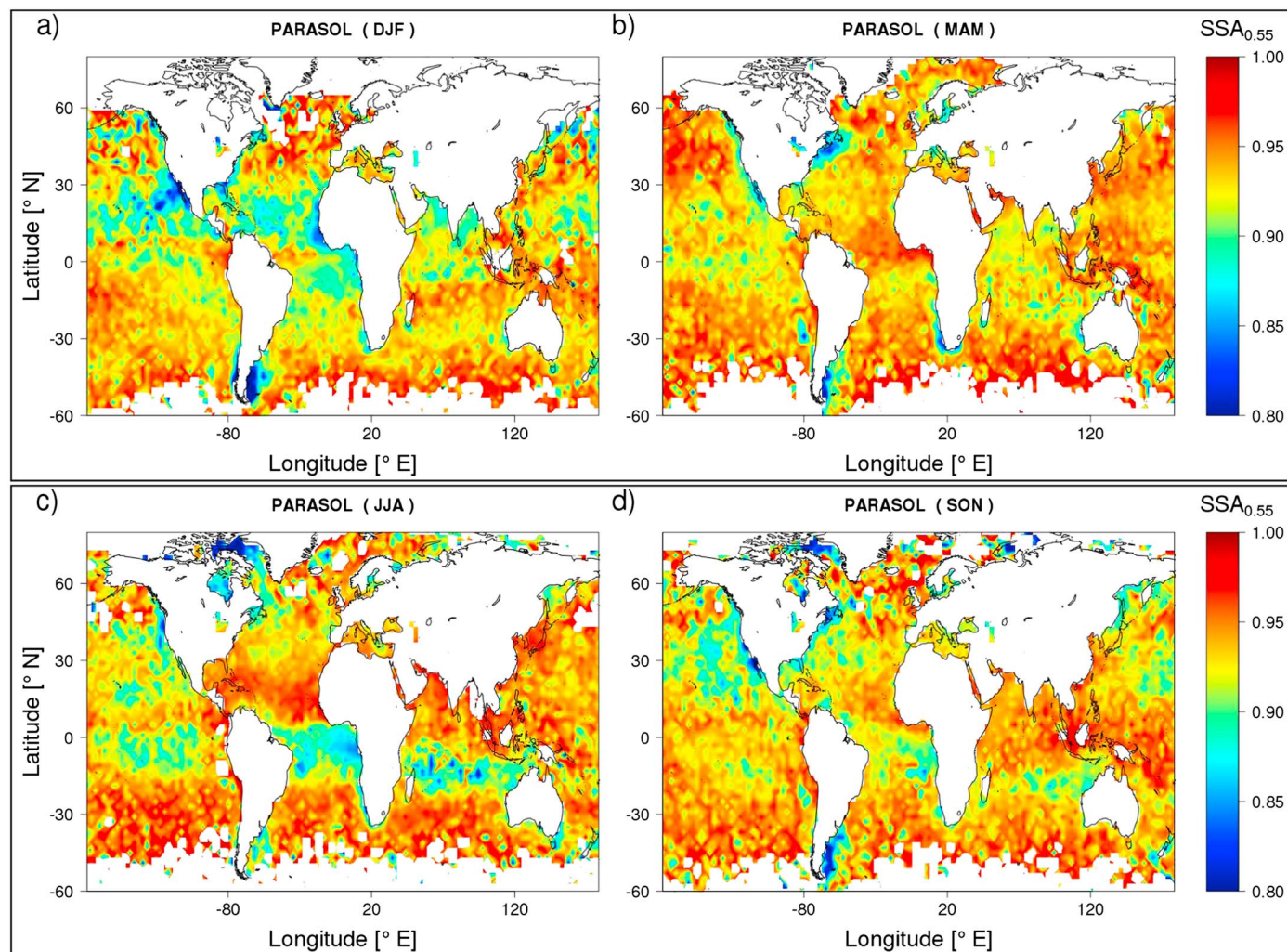


Figure 10. Seasonally averaged SSA at 0.55 μm for year 2006 from PARASOL. Grid boxes filled with less than 10 pixels in the annual mean are screened out.

(Figures 9g and 9h). A likely explanation is that models underestimate the sulfate and nitrogen load in this area, leading to lower SSA values than in PARASOL. The strong increase of these aerosol types during 2006 compared with the previous years [Zhang *et al.*, 2009; Lamsal *et al.*, 2011] may not be captured by the models.

Moreover, large disagreement also exists among the models, as shown by the zonal means of SSA, AAOD and, to a lesser extent, AOD in Figures 5c, 5f, and 5i. GOCART simulates the highest absorption values, very close to PARASOL in the Northern Hemisphere. This is partly driven by the higher absorption of dust in this model compared with observations, particularly important at the latitude of Sahara [Buchard *et al.*, 2014].

As far as AOD is concerned, models and observations show very similar patterns, with the former exhibiting lower values than the latter (Figures 9g–9i). Consistent with Kinne *et al.* [2006], AeroCom models and observations show general agreement for AOD and strong diversity for aerosol absorption.

5.1. Seasonal Variability of SSA

Seasonal maps of SSA from PARASOL and AeroCom models mean are shown in Figures 10 and 11. PARASOL reveals that low SSAs are more common during seasons December–February (DJF) and June–August (JJA) in the Northern and Southern Hemispheres, respectively (Figures 10a and 10c), while mean SSA is the highest during MAM, globally. This behavior is in agreement with the reanalysis outputs shown by Su *et al.* [2013].

AeroCom models simulate much weaker absolute seasonal variability of SSA, variations are found exclusively in close proximity to the major emission sources. Consistent with the observations, models simulate peaks of low SSAs off the coasts of central-west Africa during JJA, associated with biomass burning [Eck *et al.*, 2013].

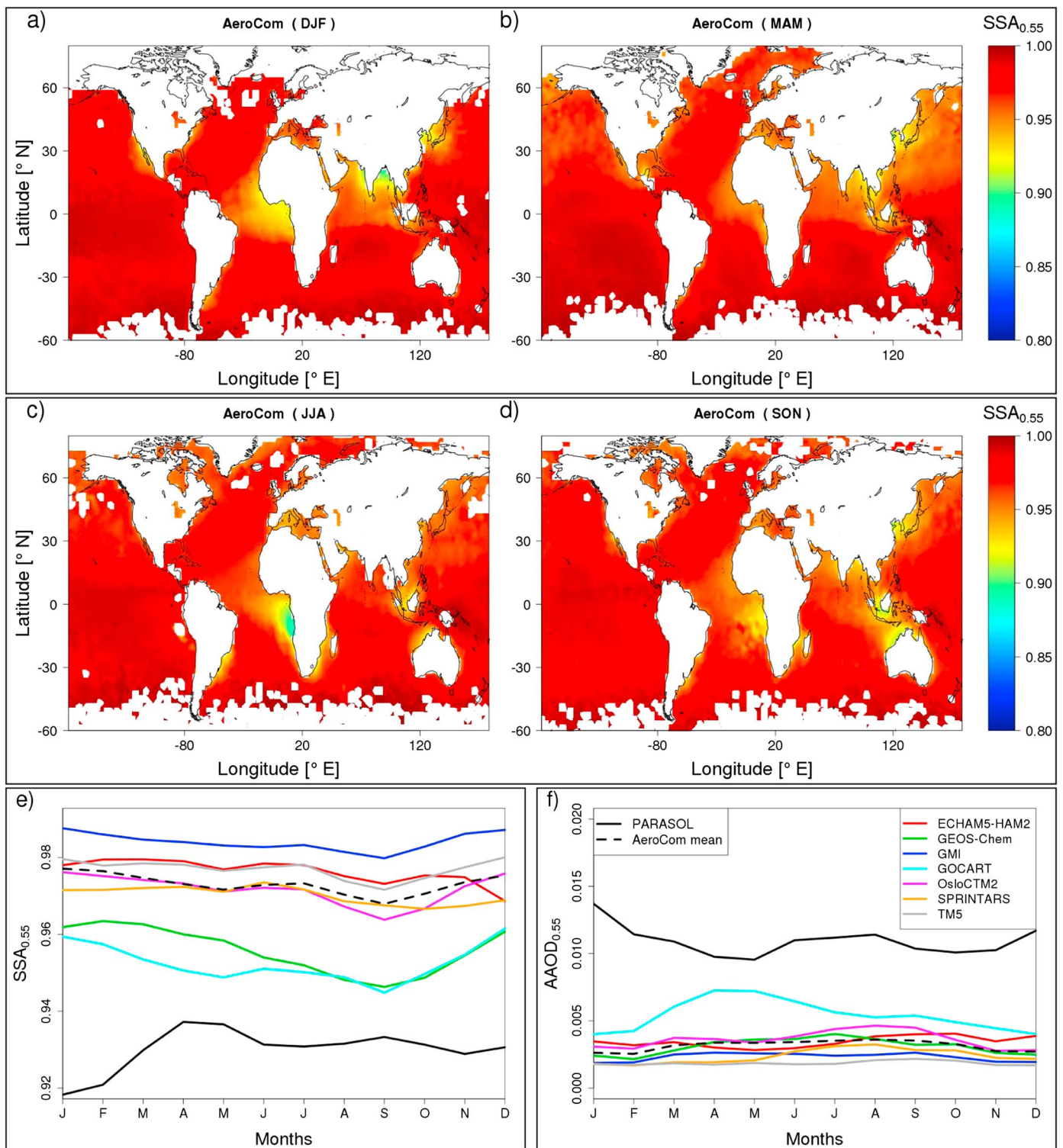


Figure 11. (a–d) Similar to Figure 10 but for the AeroCom models mean. (e–f) Monthly means (weighted by area) of SSA and AAOD from the individual AeroCom models and PARASOL.

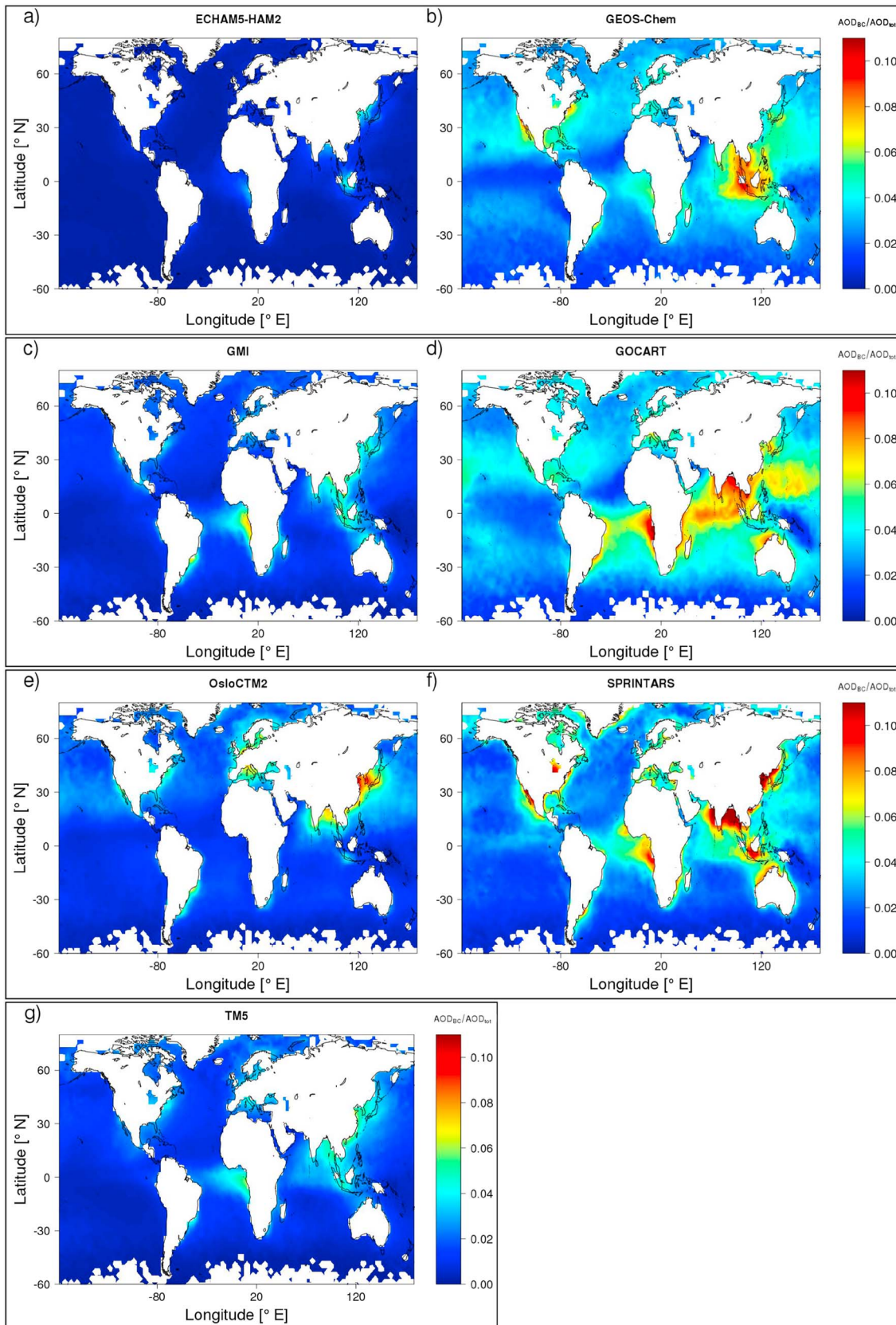


Figure 12. Annual mean of relative contribution of the black carbon aerosol component (AOD_{BC}) to the total AOD at $0.55 \mu m$, for the year 2006 from the individual AeroCom models. Note that AOD_{BC} for the OsloCTM2 model is just from fossil and biofuel components; biomass burning is not included.

Unlike PARASOL, the related SSA plume remains very close to the emission sources. The area surrounding India (Southeast Asia) experiences the lowest scattering during DJF (March–May (MAM)) both in the retrievals and in the simulations. This is in agreement with previous studies [Duncan *et al.*, 2003; Pochanart *et al.*, 2003] and is due to seasonal biomass and biofuel burning. Low-retrieved SSAs in North America during JJA can be linked to forest fires taking place when lightning strikes occur more frequently [Skinner *et al.*, 2000]. Lightning accounts for over three quarters of total area burned [Weber and Stocks, 1998]. AeroCom models simulate higher SSAs in this area, regardless of the season (Figures 10 and 11).

Other areas experience seasonal variation in aerosol scattering. For instance, the central Atlantic Ocean is characterized by biomass burning smoke from tropical Africa during boreal winters, while dust from the Sahara is present most of the year [Yu *et al.*, 2010]. Consistently, PARASOL retrieves the lowest values of SSA during DJF and higher values in the other seasons, associated with mineral dust outbreaks. During boreal spring and summer Caribbean islands are known to be influenced by dust from the Sahara [Kaufman *et al.*, 2005], which is detected by extended plumes of high SSA by PARASOL (Figure 10c). No appreciable seasonal changes in aerosol scattering are simulated by the AeroCom models for the same area. An other important aerosol location is Northeast Asia. This area is influenced by a complex mixture of particles. During DJF and MAM mineral dust mixes with the local anthropogenic pollution [Eck *et al.*, 2005]. This situation is not clear from the PARASOL SSA and may be due to retrieval errors or physical reasons discussed in section 4. In any case, AeroCom models mean SSA is characterized by very weak absolute seasonal changes. Overall, the most striking discrepancy between AeroCom and PARASOL is the different spatial and temporal variability of the absorbing aerosols in the subtropics. As discussed in the previous section, we interpret this pattern as a consequence of persistent large-scale atmospheric conditions. This is supported to a large extent by OMI-Aura observations (Figure 6a). An additional evidence of the weak absolute seasonal variability of SSA and AOD compared to the observations is shown in Figures 11e and 11f (cf. dashed and solid black lines). As for the spatial variability in the previous section, we highlight the high diversity existing among the models. The GOCART model simulates the largest temporal changes, but peaks are opposed to PARASOL.

In order to streamline the discussion, we do not describe all the regional differences between AeroCom models and PARASOL SSA. As discussed above, the observations contain a certain degree of uncertainty and some areas need further analyses for a correct interpretation of the PARASOL product (e.g., Patagonia and north Canada). On the other hand, the weak absolute variability of SSA in the models, both in terms of spatial structure and seasonal changes, appears difficult to reconcile with the satellite observations. We stress that models simulate similar seasonal values of SSA in certain areas (i.e., central Africa and India) compared with PARASOL and consistent temporal variations. However, the SSA plumes in these areas do not extend further offshore as much as in the observations. This points to deficiencies in model parameterizations over most of the oceans. These are not necessarily associated with shortcomings in the aerosol transport but could also be related to the way the optical properties are calculated. For instance, usually models assume that aerosols are externally mixed (Table 1), which may underestimate the absorption enhancement of coated BC particles. Recently, Curci *et al.* [2014] have shown that all things being equal, SSA is much lower when BC coating is considered.

Biases in modeled SSA can be the result of deficiencies in several processes. Previous studies [Kinne *et al.*, 2006; Yu *et al.*, 2010] argued that global aerosol models underestimate the contribution of tropical biomass burning smoke. Consistently, we show that the largest departures from the observations arise from the tropical belt. Bond *et al.* [2013] claimed that BC absorption is often underestimated by models, partially due to the assumed mixing state of BC [Curci *et al.*, 2014]. In addition, we find large model diversity in the BC AOD contribution to the total AOD (Figure 12) that can partially drive the intermodel diversities in SSA. This relative contribution is the largest in the GOCART and GEOS-Chem models. Moreover, Textor *et al.* [2006] pointed to the erroneous atmospheric transport and deposition of the absorbing aerosols as well as misrepresentation of water uptake as additional sources for model biases. Inappropriate inventories of the aerosol emissions used for the simulations can also lead to model departures from observations [Textor *et al.*, 2006]. Finally, biases in the imaginary part of the refractive indices can also contribute to the discrepancy between models and observations. Note that the refractive index chosen for BC in ECHAM5-HAM2 is higher than in the other models considered in this study (Table 2). However, this model does not stand out for simulating the lowest SSA among the AeroCom models (Figure 9c), partly because of the low contribution of BC AOD to the total AOD (Figure 12a).

Table 2. Refractive Index at 550 nm for Each Aerosol Species

Model	Organic Matter	Black Carbon	Mineral Dust
ECHAM5-HAM2	$1.53 + 5.5 \times 10^{-3}i$	$1.85 + 0.71i$	$1.52 + 1.1 \times 10^{-3}i$
GEOS-Chem-v822	$1.53 + 5.5 \times 10^{-3}i$	$1.75 + 0.44i$	$1.53 + 5.5 \times 10^{-3}i$
GMI	$1.53 + 6.0 \times 10^{-3}i$	$1.75 + 0.44i$	$1.53 + 5.5 \times 10^{-3}i$
GOCART-v4	$1.53 + 6.0 \times 10^{-3}i$	$1.75 + 0.44i$	$1.53 + 5.5 \times 10^{-3}i$
OsloCTM2-v2	$1.53 + 5.5 \times 10^{-3}i$	$1.75 + 0.44i$	$1.47 + 1.2 \times 10^{-3}i$
SPRINTARS-v385	$1.53 + 6.0 \times 10^{-3}i$	$1.75 + 0.44i$	$1.53 + 2.0 \times 10^{-3}i$
TM5-V3	$1.53 + 5.5 \times 10^{-3}i$	$1.75 + 0.44i$	$1.52 + 1.1 \times 10^{-3}i$

5.2. Frequency Distribution of Aerosol Optical Properties

Most of the previous findings are summarized with histograms in Figure 13. Figure 13a shows a frequency distribution histogram obtained by collecting all the daily SSA values from PARASOL and AeroCom models mean. As for the previous figures, we consider only daily model outputs where PARASOL data are available. It clearly follows from the histogram that the AeroCom models mean SSA is systematically higher than the SSA retrieved from PARASOL. Both the distributions resemble a lognormal function, with the skewness of the PARASOL distribution much more pronounced, resulting in a mean SSA of about 0.93, lower than the AeroCom mean SSA of about 0.97. The smaller range of the simulated SSA values highlights one of the limitations of bulk models: there is only one or a few types of dust and carbonaceous particles, and often only external mixtures are possible. In reality, dust from different regions have different mineralogy with varying amounts of absorptive characteristics [Prospero *et al.*, 2002]. Likewise smoke absorptive properties depend strongly on combustion phases and material burnt [Gras *et al.*, 1999]. Models specifying the same optical properties of organic carbon and dust may not capture these differences and in turn account for departures from the observed SSA.

The daily variability of the AeroCom models mean SSA (indicated by error bars) is weaker than the observed daily changes, which supports the argument that modeled SSA exhibits an overly weak temporal dependence. Figure 13a also shows the maximum and minimum global mean SSA among the AeroCom models considered (cross points). GOCART simulates SSA closer to the observations compared to the other models, in accordance with the previous findings. Results remain virtually unchanged when the small areas of unexplained features in PARASOL SSA (i.e., Patagonia and west of Greenland, see discussion in section 4) are not considered.

Positive model bias of SSA over ocean would lead to an overly negative DREA at TOA, for no bias in AOD. The radiative impact of the PARASOL-AeroCom differences can be better interpreted considering the AAOD histogram in Figure 13b. As for SSA, models underestimate the mean absorption and simulate a smaller range of AAOD values.

Since observations retrieved at low AOD have larger errors (Figure 5), we now consider only SSA values associated with daily PARASOL AOD > 0.2 in Figure 13d. AeroCom models simulations are also considered only where PARASOL AOD > 0.2. It is shown that the mean SSA in the observations does not change appreciably, but the temporal variability (denoted by error bars) is more pronounced. On the other hand, the highest AeroCom mean SSAs get less statistical weight, leading the mean SSA to get closer to the PARASOL mean. This highlights that the largest accumulated discrepancies between PARASOL and AeroCom models mean SSA occur over the open ocean, where AOD is typically small. The closer mean SSA between the two data sets is actually due to compensating positive (e.g., Guinea Gulf) and negative (e.g., Indonesian area) differences between models and observations (see Figure 9), rather than better agreement. However, when only AAOD values associated with daily PARASOL AOD > 0.2 are considered (Figure 13e), the differences between AeroCom mean and PARASOL become larger than in Figure 13b. This confirms that models underestimate aerosol absorption close to the emission sources, where AOD and DREA are more prominent.

The other important aerosol property controlling DREA is AOD. Figure 13c shows that the AeroCom models underestimate the mean AOD but much less than for AAOD (in a relative sense). The multimodel distribution resembles closely the distribution depicted by PARASOL. In particular, the ECHAM5-HAM2 model simulates AOD values very close to the observations, in agreement with Zhang *et al.* [2012]. Our findings, in terms of

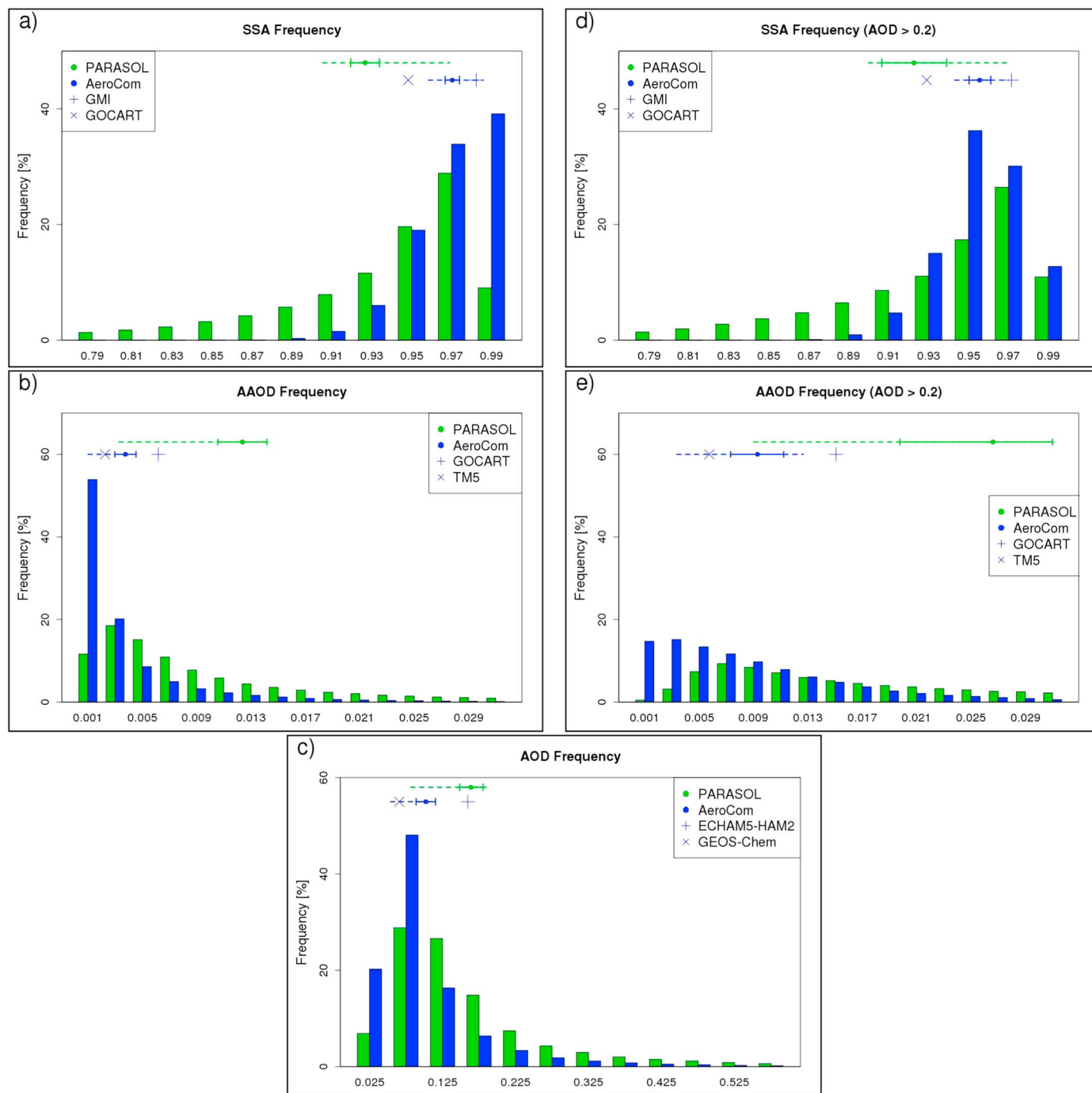


Figure 13. Frequency of occurrence (expressed in %) of daily (a) SSA, (b) AAOD, and (c) AOD at 0.55 μm for each bin during 2006. Dots represent the global mean (weighted by area), along with 1σ standard deviation of the daily variability, dashed lines end with the 25th and 75th percentiles of the distributions. Cross points represent the mean quantity from the model with the highest or smallest global mean among the AeroCom models considered. (d and e) Similar to Figures 13a and 13b, respectively, but only daily values associated with daily PARASOL AOD > 0.2 are considered.

similar AOD and significant discrepancy in AAOD and SSA between models and observations, are consistent with and expand *Kinne et al.'s* [2006] results. They showed that despite the general agreement in total AOD among models and between models and observations, AeroCom models exhibit large diversities in the simulated AOD from the individual tracers. This reveals relevant intermodel differences in the partitioning between scattering and absorbing aerosol components, which is brought out when SSA is analyzed.

6. Summary and Discussion

Despite aerosol SSA being the biggest contributor to the total uncertainty in DREA, accurate measurement of this quantity remains challenging [Remer *et al.*, 2009]. A recent effort aiming at providing global coverage SSA is based on multiangle multispectral photopolarimetric measurements from the PARASOL microsatellite [Hasekamp *et al.*, 2011]. In this study we presented the first global ocean comparison of aerosol optical properties from PARASOL with other observations and model simulations.

In order to ensure correct interpretation of the results, we evaluated the novel PARASOL data set against ground-based AERONET observations. The majority of the SSA, AAOD, and AOD retrievals is within 0.05 of the AERONET measurements. Given the uncertainty in AERONET, the comparison shows rather robust performance of the algorithm employed. An accurate validation of satellite inversions over ocean is challenging, because of the very few coincident events meeting the AERONET high AOD (> 0.4) criterion to obtain a completely satisfactory sampling of SSA retrievals. Future validations with longer time series than the single year (2006) used in this study would help to acquire better statistics.

In order to get more insights into PARASOL SSA, we compared global distribution maps with an other independent data set with larger spatial coverage than AERONET, namely, the OMI-Aura satellite observations. The two space-based measurements exhibit consistent patterns, both reveal the rich structure of SSA, due to local differences in the aerosol composition. The highest SSAs are detected in the Southern Ocean at extratropical latitudes, where sea salt is dominant. In contrast, lower values are found west of the continents in the subtropics. This appears related to persistent large-scale circulation conditions, such as those associated with the trade winds, leading absorbing aerosol plumes to substantially influence SSA also far away from their emission sources. Along the intertropical convergence zones, SSA rises to higher values, likely associated with the strong water uptake taking place in these humid environments, typical of deep convective regimes.

Although the novel PARASOL product successfully provides a consistent and representative signal of the mean regional SSA, AAOD, and AOD, compared with AERONET and OMI-Aura, some unexpected results were identified. Namely, west of Greenland and close to Patagonia, where PARASOL detects remarkably low SSAs. Sensitivity tests and exploratory work motivated by these findings are underway and will be reported separately.

In the second part of this study, SSA and AAOD from polarimetric measurements over the ocean, available for the first time, were compared with global aerosol models, participating in the AeroCom project. Although models are continuously improved, the simulations analyzed represent the most recent data available for an intercomparison study of global aerosol models. The model versions correspond to 2012 state of the art, as used for the recent forcing estimate from AeroCom phase II in Myhre *et al.* [2013a]. Despite some models comparing better than others, the spatial distribution of the simulated SSA is rather uniform and higher, contrasted with the PARASOL observations. Lower values are found in the area over Indonesia and off the coasts of China. Furthermore, high diversity in magnitude and spatial pattern of SSA exists among the models, with GOCART simulating the highest absorption. Such a diversity is partially due to intermodel differences in simulating the BC AOD contribution to the total AOD.

At the seasonal scale, changes in PARASOL SSA are found highly consistent with the expected variability of fire events and dust outbreaks, contributing to build confidence in the novel product. On the other hand, the AeroCom models simulate much weaker absolute seasonal changes in SSA; variations are found exclusively in close proximity to the major emission sources. Overall, the models simulate much weaker absolute variability of SSA compared with observations, both in terms of spatial structure and seasonal changes.

The radiative impact of these PARASOL-AeroCom differences can be better interpreted by inspecting the AAOD maps. Satellite retrievals attest stronger aerosol absorption than the models at all latitudes, with larger discrepancies in the tropics. At the regional scale, these differences can be either positive or negative. As far as the observational uncertainties are concerned, analyses of maps of AAOD are reassuring. Because they show that the largest PARASOL-AeroCom differences, in terms of magnitude and spatial extension, origin primarily from the Gulf of Guinea, an area not associated with unexpected features in PARASOL SSA (i.e., Patagonia and west of Greenland). From a radiative transfer perspective this is important, because AAOD reveals largely where the SSA discrepancies are relevant for DREA.

The other important factor controlling the aerosol radiative forcing is AOD. The AeroCom models simulate AOD values similar, or slightly underestimated, to the observations, in agreement with previous studies [e.g., Kinne *et al.*, 2006]. Slightly underestimated AOD and overestimated SSA compensate to a certain extent the biases in the modeled DREA. However, sensitivity experiments demonstrate that SSA uncertainties are the leading factor affecting DREA calculations [Loeb and Su, 2010]. This evidence along with our findings suggest that current model estimates of DREA strength at TOA are biased high over most of the oceans. In addition, since DREA at the surface is enhanced at low SSA values, the aerosol cooling effect at the surface is likely underestimated in the models. This implies that aerosols exert larger direct and semidirect effects within the atmosphere to alter the atmospheric circulation, cloud processes and the water cycle than currently estimated by models. Given the consistency between PARASOL, AERONET, and OMI-Aura, it is most likely that these conclusions reflect model biases rather than observational uncertainties. Future analyses with radiative transfer calculations are needed to quantify and explore further the impact of these biases on the Earth's climate system.

According to Remer *et al.* [2009], SSA needs to be much better represented in models through improving the estimates of carbonaceous and dust aerosol sources, their atmospheric distributions, and optical properties. In this respect, any effort to retrieve SSA for model evaluation deserves attention. Apart from relatively minor issues, the present analyses showed very encouraging results from the PARASOL observations. Certain regions demand further refinement to increase the confidence and credibility of the novel aerosol product. The PARASOL-based data set is currently under development to include retrievals over land and may constitute the basis for the regional to global scale assessment of atmospheric models, thereby improving and constraining simulations of key aerosol parameters.

Acknowledgments

This work has been supported by the User Support Space Research program of the Netherlands Organization for Scientific Research (NWO) through project ALW-GO/13-38. The authors are grateful to the three anonymous reviewers for their constructive comments that have helped the improvement of this paper. We thank the AERONET principal investigators and their staff for establishing and maintaining the sites used in this study. The AERONET data set can be obtained from <http://aeronet.gsfc.nasa.gov/>. We thank NASA-GES-DISC for the online availability of the OMI aerosol products at http://disc.sci.gsfc.nasa.gov/Aura/data-holdings/OMI/omaeruv_v003. The AeroCom data can be accessed following the instructions at <http://aerocom.met.no/data.html>. The PARASOL data set, the results, and the code used in this study are available at <https://owncloud.sron.nl/owncloud/index.php/s/057KmaAolfN5sn7>, pending an e-mail request to C.Lacagnina@sron.nl.

References

- Abel, S. J., J. M. Haywood, E. J. Highwood, J. Li, and P. R. Buseck (2003), Evolution of biomass burning aerosol properties from an agricultural fire in southern Africa, *Geophys. Res. Lett.*, *30*(15), 1783, doi:10.1029/2003GL017342.
- Bey, I., D. J. Jacob, R. M. Yantosca, J. A. Logan, B. D. Field, A. M. Fiore, Q. Li, H. Y. Liu, L. J. Mickley, and M. G. Schultz (2001), Global modeling of tropospheric chemistry with assimilated meteorology: Model description and evaluation, *J. Geophys. Res.*, *106*(D19), 23,073–23,095, doi:10.1029/2001JD000807.
- Bond, T. C., et al. (2013), Bounding the role of black carbon in the climate system: A scientific assessment, *J. Geophys. Res. Atmos.*, *118*(11), 5380–5552, doi:10.1002/jgrd.50171.
- Buchard, V., A. M. da Silva, P. R. Colarco, A. Darmenov, C. A. Randles, R. Govindaraju, O. Torres, J. Campbell, and R. Spurr (2014), Using the OMI aerosol index and absorption aerosol optical depth to evaluate the NASA MERRA Aerosol Reanalysis, *Atmos. Chem. Phys. Discuss.*, *14*(23), 32,177–32,231.
- Cazorla, A., R. Bahadur, K. J. Suski, J. F. Cahill, D. Chand, B. Schmid, V. Ramanathan, and K. A. Prather (2013), Relating aerosol absorption due to soot, organic carbon, and dust to emission sources determined from in-situ chemical measurements, *Atmos. Chem. Phys.*, *13*(18), 9337–9350.
- Chen, W.-T., R. Kahn, D. N. Elson, K. Yau, and J. Seinfeld (2008), Sensitivity of multi-angle imaging to optical and microphysical properties of biomass burning aerosols, *J. Geophys. Res.*, *113*, D10203, doi:10.1029/2007JD009414.
- Chin, M., R. B. Rood, S.-J. Lin, J.-F. Müller, and A. M. Thompson (2000), Atmospheric sulfur cycle simulated in the global model GOCART: Model description and global properties, *J. Geophys. Res. Atmos.*, *105*(D20), 24,671–24,687.
- Chowdhary, J., B. Cairns, M. Mishchenko, and L. Travis (2001), Retrieval of aerosol properties over the ocean using multispectral and multiangle photopolarimetric measurements from the Research Scanning Polarimeter, *Geophys. Res. Lett.*, *28*(2), 243–246.
- Curci, G., et al. (2014), Uncertainties of simulated aerosol optical properties induced by assumptions on aerosol physical and chemical properties: An AQMEII-2 perspective, *Atmos. Environ.*, *115*, 541–552.
- Dee, D. P., et al. (2011), The ERA-Interim reanalysis: Configuration and performance of the data assimilation system, *Q. J. R. Meteorol. Soc.*, *137*(656), 553–597.
- Deschamps, P.-Y., F.-M. Breon, M. Leroy, A. Podaire, A. Bricaud, J.-C. Buriez, and G. Seze (1994), The POLDER mission: Instrument characteristics and scientific objectives, *IEEE Trans. Geosci. Remote Sens.*, *32*(3), 598–615.
- Dubovik, O., and M. D. King (2000), A flexible inversion algorithm for retrieval of aerosol optical properties from Sun and sky radiance measurements, *J. Geophys. Res.*, *105*, 20,673–20,696.
- Dubovik, O., A. Smirnov, B. N. Holben, M. D. King, Y. J. Kaufman, T. F. Eck, and I. Slutsker (2000), Accuracy assessments of aerosol optical properties retrieved from Aerosol Robotic Network (AERONET) Sun and sky radiance measurements, *J. Geophys. Res. Atmos.*, *105*(D8), 9791–9806.
- Dubovik, O., B. N. Holben, Y. J. Kaufman, M. Yamasoe, A. Smirnov, D. Tanré, and I. Slutsker (2011), Single-scattering albedo of smoke retrieved from the sky radiance and solar transmittance measured from ground, *J. Geophys. Res.*, *4*, 31,903–31,923, doi:10.1029/98JD02276.
- Duncan, B. N., R. V. Martin, A. C. Staudt, R. Yevich, and J. A. Logan (2003), Interannual and seasonal variability of biomass burning emissions constrained by satellite observations, *J. Geophys. Res.*, *108*(D2), 4100, doi:10.1029/2002JD002378.
- Eck, T. F., et al. (2005), Columnar aerosol optical properties at AERONET sites in central eastern Asia and aerosol transport to the tropical mid-Pacific, *J. Geophys. Res.*, *110*, D06202, doi:10.1029/2004JD005274.
- Eck, T. F., et al. (2013), A seasonal trend of single scattering albedo in southern African biomass-burning particles: Implications for satellite products and estimates of emissions for the world's largest biomass-burning source, *J. Geophys. Res. Atmos.*, *118*, 6414–6432, doi:10.1002/jgrd.50500.
- French, N. H. F., E. S. Kasichke, R. J. Hall, K. A. Murphy, D. L. Verbyla, E. E. Hoy, and J. L. Allen (2008), Using Landsat data to assess fire and burn severity in the North American boreal forest region: An overview and summary of results, *Int. J. Wildland Fire*, *17*, 443–462.

- Ginoux, P., J. M. Prospero, O. Torres, and M. Chin (2004), Long-term simulation of global dust distribution with the GOCART model: Correlation with North Atlantic Oscillation, *Environ. Model. Software*, *19*(2), 113–128.
- Gras, J. L., J. B. Jensen, K. Okada, M. Ikegami, Y. Zaizen, and Y. Makino (1999), Some optical properties of smoke aerosol in Indonesia and tropical Australia, *Geophys. Res. Lett.*, *26*(10), 1393–1396.
- Hansen, J., M. Sato, and R. Ruedy (1997), Radiative forcing and climate response, *J. Geophys. Res.*, *102*, 6831–6864.
- Hasekamp, O. P., and J. Landgraf (2007), Retrieval of aerosol properties over land surfaces: Capabilities of multiple-viewing-angle intensity and polarization measurements, *Appl. Opt.*, *46*(16), 3332–3344.
- Hasekamp, O. P., P. Litvinov, and A. Butz (2011), Aerosol properties over the ocean from PARASOL multiangle photopolarimetric measurements, *J. Geophys. Res. Atmos.*, *116*, D14204, doi:10.1029/2010JD015469.
- Holben, B. N., et al. (2001), An emerging ground-based aerosol climatology: Aerosol optical depth from AERONET, *J. Geophys. Res.*, *106*(D11), 12,067–12,097.
- Jethva, H., O. Torres, and C. Ahn (2014), Global assessment of OMI aerosol single-scattering albedo using ground-based AERONET inversion, *J. Geophys. Res. Atmos.*, *119*, 9020–9040, doi:10.1002/2014JD021672.
- Johnson, B. T., S. Christopher, J. M. Haywood, S. R. Osborne, S. McFarlane, C. Hsu, C. Salustro, and R. Kahn (2009), Measurements of aerosol properties from aircraft, satellite and ground-based remote sensing: A case-study from the Dust and Biomass-burning Experiment (DABEX), *Q. J. R. Meteorol. Soc.*, *135*, 922–934.
- Kahn, R. A., B. J. Gaitley, J. V. Martonchik, D. J. Diner, K. A. Crean, and B. Holben (2005), Multiangle Imaging Spectroradiometer (MISR) global aerosol optical depth validation based on 2 years of coincident Aerosol Robotic Network (AERONET) observations, *J. Geophys. Res. Atmos.*, *110*, D10S04, doi:10.1029/2004JD004706.
- Kahn, R. A., B. J. Gaitley, M. J. Garay, D. J. Diner, T. Eck, A. Smirnov, and B. N. Holben (2010), Multiangle Imaging Spectroradiometer global aerosol product assessment by comparison with the Aerosol Robotic Network, *J. Geophys. Res.*, *115*, D23209, doi:10.1029/2010JD014601.
- Kaufman, Y. J., I. Koren, L. A. Remer, D. Tanré, P. Ginoux, and S. Fan (2005), Dust transport and deposition observed from the Terra-Moderate Resolution Imaging Spectroradiometer (MODIS) spacecraft over the Atlantic Ocean, *J. Geophys. Res. Atmos.*, *110*, D10S12, doi:10.1029/2003JD004436.
- Kinne, S., et al. (2006), An AeroCom initial assessment—Optical properties in aerosol component modules of global models, *Atmos. Chem. Phys.*, *6*(7), 1815–1834.
- Lacagnina, C., and F. Selten (2013), Changes in the cloud properties in response to El Niño: A bivariate approach, *Clim. Dyn.*, *40*(11–12), 2973–2991.
- Lamsal, L. N., R. V. Martin, A. Padmanabhan, A. van Donkelaar, Q. Zhang, C. E. Sioris, K. Chance, T. P. Kurosu, and M. J. Newchurch (2011), Application of satellite observations for timely updates to global anthropogenic NO_x emission inventories, *Geophys. Res. Lett.*, *38*, L05810, doi:10.1029/2010GL046476.
- Leahy, L. V., T. L. Anderson, T. F. Eck, and R. W. Bergstrom (2007), A synthesis of single scattering albedo of biomass burning aerosol over southern Africa during SAFARI 2000, *Geophys. Res. Lett.*, *34*, L12814, doi:10.1029/2007GL029697.
- Liu, X., J. E. Penner, B. Das, D. Bergmann, J. M. Rodriguez, S. Strahan, M. Wang, and Y. Feng (2007), Uncertainties in global aerosol simulations: Assessment using three meteorological data sets, *J. Geophys. Res. Atmos.*, *112*, D11212, doi:10.1029/2006JD008216.
- Loeb, N. G., and N. Manalo-Smith (2005), Top-of-Atmosphere direct radiative effect of aerosols over global oceans from merged CERES and MODIS observations, *J. Clim.*, *18*, 3506–3526.
- Loeb, N. G., and W. Su (2010), Direct aerosol radiative forcing uncertainty based on a radiative perturbation analysis, *J. Clim.*, *23*, 5288–5293.
- Mallet, M., O. Dubovik, P. Nabat, F. Dulac, R. Kahn, J. Sciare, D. Paronis, and J. F. Léon (2013), Absorption properties of Mediterranean aerosols obtained from multi-year ground-based remote sensing observations, *Atmos. Chem. Phys.*, *13*(18), 9195–9210.
- Mishchenko, M. I., and L. D. Travis (1997), Satellite retrieval of aerosol properties over the ocean using polarization as well as intensity of reflected sunlight, *J. Geophys. Res.*, *102*(D14), 16,989–17,013.
- Myhre, G., N. Belloin, T. F. Berglen, T. K. Berntsen, O. Boucher, A. Grini, I. S. A. Isaksen, M. Johnsrud, M. I. Mishchenko, F. Stordal, and D. Tanré (2007), Comparison of the radiative properties and direct radiative effect of aerosols from a global aerosol model and remote sensing data over ocean, *Tellus B*, *59*(1), 115–129.
- Myhre, G., et al. (2009), Modelled radiative forcing of the direct aerosol effect with multi-observation evaluation, *Atmos. Chem. Phys.*, *9*(4), 1365–1392.
- Myhre, G., et al. (2013a), Radiative forcing of the direct aerosol effect from AeroCom Phase II simulations, *Atmos. Chem. Phys.*, *13*, 1853–1877.
- Myhre, G., et al. (2013b), Anthropogenic and natural radiative forcing, in *Climate Change 2013: The Physical Science Basis. Contribution of Working Group I to the Fifth Assessment Report of the Intergovernmental Panel on Climate Change*, edited by T. F. Stocker et al., pp. 659–740, Cambridge Univ. Press, Cambridge, U. K., and New York.
- Osborne, S. R., B. T. Johnson, J. M. Haywood, A. J. Baran, M. A. J. Harrison, and C. L. McConnell (2008), Physical and optical properties of mineral dust aerosol during the Dust and Biomass-burning Experiment, *J. Geophys. Res. Atmos.*, *113*, D00C03, doi:10.1029/2007JD009551.
- Pochanart, P., H. Akimoto, Y. Kajii, and P. Sukasem (2003), Carbon monoxide, regional-scale transport, and biomass burning in tropical continental Southeast Asia: Observations in rural Thailand, *J. Geophys. Res. Atmos.*, *108*(D17), 4552, doi:10.1029/2002JD003360.
- Prospero, J. M., P. Ginoux, O. Torres, S. E. Nicholson, and T. E. Gill (2002), Environmental characterization of global sources of atmospheric soil dust identified with the nimbus 7 Total Ozone Mapping Spectrometer (TOMS) absorbing aerosol product, *Rev. Geophys.*, *40*(1), 1002, doi:10.1029/2000RG000095.
- Remer, L. A., et al. (2009), *Executive Summary. Atmospheric Aerosol Properties and Climate Impacts—A Report by the U.S. Climate Change Science Program and the Subcommittee on Global Change Research*, edited by M. Chin, R. A. Kahn, and S. E. Schwartz, National Aeronautics and Space Administration, Washington, D. C.
- Russell, P. B., et al. (2002), Comparison of aerosol single scattering albedos derived by diverse techniques in two North Atlantic experiments, *J. Atmos. Sci.*, *59*, 609–619.
- Russell, P. B., et al. (2014), A multiparameter aerosol classification method and its application to retrievals from spaceborne polarimetry, *J. Geophys. Res. Atmos.*, *119*(16), 9838–9863, doi:10.1002/2013JD021411.
- Sayer, A. M., N. C. Hsu, T. F. Eck, A. Smirnov, and B. N. Holben (2014), AERONET-based models of smoke-dominated aerosol near source regions and transported over oceans, and implications for satellite retrievals of aerosol optical depth, *Atmos. Chem. Phys.*, *14*(20), 11,493–11,523.
- Schafer, J. S., et al. (2014), Intercomparison of aerosol single-scattering albedo derived from AERONET surface radiometers and LARGE in situ aircraft profiles during the 2011 DRAGON-MD and DISCOVER-AQ experiments, *J. Geophys. Res. Atmos.*, *119*, 7439–7452, doi:10.1002/2013JD021166.
- Schulz, M., M. Chin, and S. Kinne (2009), *The Aerosol Model Comparison Project, AeroCom, Phase II: Clearing Up Diversity*, IGAC Newsletter N 41, 2–11.

- Skinner, W. R., B. J. Stocks, D. L. Martell, B. Bonsal, and A. Shabbar (2000), The relationship between area burned by wildland fire in Canada and circulation anomalies in the mid-troposphere, in *Biomass Burning and Its Inter-Relationships With the Climate System*, vol. 3, pp. 101–125, Springer, Netherlands.
- Stap, F. A., O. Hasekamp, and T. Röckmann (2014), Sensitivity of PARASOL multi-angle photo-polarimetric aerosol retrievals to cloud contamination, *Atmos. Meas. Tech. Discuss.*, *7*(10), 10,673–10,714.
- Su, W., N. G. Loeb, G. L. Schuster, M. Chin, and F. G. Rose (2013), Global all-sky shortwave direct radiative forcing of anthropogenic aerosols from combined satellite observations and GOCART simulations, *J. Geophys. Res. Atmos.*, *118*(2), 655–669, doi:10.1029/2012JD018294.
- Takemura, T., T. Nozawa, S. Emori, T. Y. Nakajima, and T. Nakajima (2005), Simulation of climate response to aerosol direct and indirect effects with aerosol transport-radiation model, *J. Geophys. Res. Atmos.*, *110*, D02202, doi:10.1029/2004JD005029.
- Tanré, D., F. M. Bréon, J. L. Deuzé, O. Dubovik, F. Ducos, P. François, P. Goloub, M. Herman, A. Lifermann, and F. Waquet (2011), Remote sensing of aerosols by using polarized, directional and spectral measurements within the A-Train: The PARASOL mission, *Atmos. Meas. Tech.*, *4*(7), 1383–1395.
- Textor, C., et al. (2006), Analysis and quantification of the diversities of aerosol life cycles within AeroCom, *Atmos. Chem. Phys.*, *6*(7), 1777–1813.
- Torres, O., C. Ahn, and Z. Chen (2013), Improvements to the OMI near-UV aerosol algorithm using A-train CALIOP and AIRS observations, *Atmos. Meas. Tech.*, *6*(11), 3257–3270.
- van Noije, T. P. C., P. Le Sager, A. J. Segers, P. F. J. van Velthoven, M. C. Krol, W. Hazeleger, A. G. Williams, and S. D. Chambers (2014), Simulation of tropospheric chemistry and aerosols with the climate model EC-Earth, *Geosci. Model Dev.*, *7*(5), 2435–2475.
- Veihelmann, B., P. F. Levelt, P. Stammes, and J. P. Veefkind (2007), Simulation study of the aerosol information content in OMI spectral reflectance measurements, *Atmos. Chem. Phys.*, *7*(12), 3115–3127.
- Weber, M. G., and B. J. Stocks (1998), Forest fires and sustainability in the boreal forests of Canada, *Ambio*, *27*(7), 545–550.
- Yang, Z., J. Wang, C. Ichoku, E. Hyer, and J. Zeng (2013), Mesoscale modeling and satellite observation of transport and mixing of smoke and dust particles over northern sub-Saharan African region, *J. Geophys. Res. Atmos.*, *118*(21), 12,139–12,157, doi:10.1002/2013JD020644.
- Yu, H., M. Chin, D. M. Winker, A. H. Omar, Z. Liu, C. Kittaka, and T. Diehl (2010), Global view of aerosol vertical distributions from CALIPSO lidar measurements and GOCART simulations: Regional and seasonal variations, *J. Geophys. Res. Atmos.*, *115*, D00H30, doi:10.1029/2009JD013364.
- Zhang, Q., et al. (2009), Asian emissions in 2006 for the NASA INTEX-B mission, *Atmos. Chem. Phys.*, *9*(14), 5131–5153.
- Zhang, K., et al. (2012), The global aerosol-climate model ECHAM-HAM, version 2: Sensitivity to improvements in process representations, *Atmos. Chem. Phys.*, *12*(19), 8911–8949.